Geosci. Model Dev. Discuss., https://doi.org/10.5194/gmd-2017-217
Manuscript under review for journal Geosci. Model Dev.
Discussion started: 26 October 2017

Geoscientific Model Development
Discussions
Open Access

Numerical experiments on isotopic diffusion in polar snow and firn using a multi-layer energy balance model

Alexandra Touzeau[1], Amaëlle Landais[1], Samuel Morin[2], Laurent Arnaud[3], Ghislain Picard[3]

[1]LSCE, CNRS UMR8212, UVSQ, Université Paris-Saclay, Gif-sur-Yvette, 91191, France
[2]Météo-France - CNRS, CNRM UMR3589, Centre d'Etudes de la Neige, Grenoble, France
[3]LGGE, CNRS UMR5183, Université Grenoble Alpes, Grenoble, France

Correspondence to: Alexandra Touzeau (alexandra.touzeau@lsce.ipsl.fr)

Abstract.

To evaluate the impact of vapor diffusion onto isotopic composition variations in the snow pits and then in ice cores, we introduced water isotopes in the detailed snowpack model Crocus. The isotopes routine is run with a 1 s resolution. At each step and for each snow layer, 1) the initial isotopic composition of vapor is taken at equilibrium with solid phase, 2) kinetic fractionation is applied during transport, and 3) condensation is realized.

We study the different effects of temperature gradient, compaction, wind compaction and precipitation on the final vertical isotopic profiles. We also run complete simulations of vapor and isotopic diffusion at GRIP, Greenland and at Dome C, Antarctica over periods of 1 or 10 years. The vapor diffusion tends to smooth the original seasonal signal, with an attenuation of 9.5% of the original signal over 10 years at GRIP. This is smaller than the observed attenuation in ice cores, indicating that the model underestimates attenuation due to diffusion or that other processes, such as ventilation, also contribute to the observed attenuation. At Dome C, the attenuation is stronger (14 %), probably because of the lower accumulation and stronger $\delta^{18}O$ gradients.

Because vapor diffusion is not the only process responsible of the signal attenuation, it would be useful to implement in the model ventilation of the snowpack and exchanges with the atmosphere to evaluate their contribution.

1 Introduction

Ice is a key archive for past climate reconstruction, which preserves both the composition of the past atmosphere in bubbles (EPICA comm. members, 2004; Kawamura et al., 2007; Petit et al., 1999; Schilt et al., 2010) and indications relevant to the temperature of formation of the snow precipitation through variations of the isotopic ratio of oxygen or deuterium (EPICA comm. members, 2004; Johnsen et al., 1995; Jouzel et al., 2007; Kawamura et al., 2007; Lorius et al., 1985; Petit et al., 1999; Schneider et al., 2006; Stenni et al., 2004). This archive is particularly useful in the southern hemisphere, where continental archives are rare (Mann and Jones, 2003; Mayewski and Goodwin, 1999). In Antarctica, where meteorological records only started in the 50's (Genthon et al., 2013), these archives are not only a tool for past climate reconstruction, but also a necessary source of information for understanding climate variability (Ekaykin et al., 2014; EPICA comm. members, 2006; Jouzel et al., 2007; Jouzel et al., 2005; Masson-Delmotte et al., 2003; Shaheen et al., 2013; Steig, 2006; Stenni et al., 2011; Stenni et al., 2004) and recent climate change (Altnau et al., 2015; Joos and Spahni, 2008; Mann and Jones, 2003; Mayewski and Goodwin, 1999; Schneider et al., 2006).

When using ice cores for past climate reconstruction, other parameters than temperature at condensation influence the isotopic compositions and must be considered. Humidity and temperature in the region of evaporation (Landais et al., 2008; Masson-Delmotte et al., 2011; Vimeux et al., 2002), or the seasonality of precipitation (Delmotte et al., 2000; Sime et al., 2008; Laepple et al., 2011) should be taken into account. In addition, uneven accumulation in time and space introduces randomness in the core stratigraphy ('stratigraphic noise', Ekaykin et al., 2009). Indeed, records from adjacent snow pits have been shown to be markedly different, under the influence of decameter-scale local effects (wind redeposition of snow, erosion, compaction, metamorphism) (Casado et al., 2016b; Ekaykin et al., 2014; Ekaykin et al., 2002; Petit et al., 1982). These local effects reduce the signal /noise ratio, and then only stacking a series of snow pits can eliminate this local variability and yield information relevant to recent climate variations (Altnau et al., 2015; Ekaykin et al., 2014; Ekaykin et al., 2002; Fisher and Koerner, 1994; Hoshina et al., 2014). This concern is particularly significant in central regions of east Antarctica characterized by very low accumulation rates (< 100 mm w.e. per year, van de Berg et al., 2006) and strong winds which can scour and erode snow layer over depths larger than the annual accumulation (Frezzotti et al., 2005; Libois et al., 2014; Morse et al., 1999; Magand et al., 2004; Epstein and Sharp, 1965; Town et al., 2008, Picard et al., 2016). There is thus a strong need to study post-deposition effects in these cold and dry regions.

Additionally to mechanical shuffling of the snow, the isotopic compositions are further modified in the snowpack. First, diffusion against isotopic gradients can occur within the ice microstructure at solid state ('solid diffusion', Ramseier et al., 1967). Second, within the porosity, the vapor isotopic composition can change due to diffusion against isotopic gradients (in gaseous state), oriented vapor transport caused by vapor density gradients, ventilation (also in gaseous state), or exchanges between the gas phase and the solid phase (sublimation, condensation). The combination of diffusion against isotopic gradients in the vapor and of exchange between vapor and the solid phase has been suggested to be the main explanation to the smoothing of the isotopic signal in the solid phase (Johnsen et al., 2000; Gkinis et al., 2014). The combination of oriented vapor transport caused by vapor density gradients and exchange with the solid phase ('dry metamorphism', Colbeck et al., 1983), or by snow ventilation and exchange with the solid phase ('forced ventilation', Town et al., 2008) also modifies the isotopic compositions in the solid phase, but in a less predictable way. Last, at the top of the snowpack, the isotopic composition of snow may also be modified through direct exchange with atmospheric vapor (Casado et al., 2016b; Ritter et al., 2016).

To elucidate the impact of these various post-deposition processes on the snow isotopic compositions, numerical models are powerful tools, since they allow discriminating between processes and test their impact one at a time. Indeed, Johnsen et al. (2000) have been able to simulate and deconvolute the influence of diffusion against isotopic gradients in the vapor at GRIP and NGRIP using a numerical model. To do this, they evaluated the diffusion length (as a function of depth) using a deformation model and an equation of diffusivity of the water isotopes in snow. This diffusion length is then used to compute the attenuation ratio (A/Ao), and in the end retrieve the original amplitude (Ao). Additionaly, the effect of forced ventilation was investigated by Neumann (2003) and Town et al. (2008) using similar multi-layer numerical models. In these models, wind-driven ventilation forces atmospheric vapor into snow; there, the vapor is condensed especially in layers colder than the atmosphere.

We focus on the impact of oriented vapor transport caused by vapor density gradients in the snow and recrystalization (i.e. 'dry metamorphism') and of diffusion against isotopic gradients. Because the vapor density gradients directly result from temperature gradients within the snowpack, the first prerequisite of our model is to correctly simulate macroscopic energy transfer within the snowpack and energy exchange at the surface. The second prerequisite is that the model includes a description of the snow microstructure, because exchanges between vapor and solid grains depend on it and its evolution in time. Snow microstructure is typically represented by its emerging scalar properties such as density, specific surface area and higher order terms often referred to as “shape parameters” (e.g. Krol and Löwe, 2016). While the concept of “grain” bears ambiguity, it is a widely used term in snow science and glaciology which we here employ as a surrogate for “elementary microstructure element”, without explicit reference to a formal definition, be it crystallographic or geometrical.

Crocus is a unidimensional multi-layer model of snowpack with a typically centimetric resolution initially dedicated to the numerical simulation of snow in temperate regions (Brun et al., 1992). It describes dry snow metamorphism (evolution of the snow microstructure) driven by temperature and temperature gradients, using semi-empirical variables and laws. It has been used for ice-sheet conditions in polar regions, both Greenland and Antarctica (Brun et al., 2011; Lefebre et al., 2003; Fréville et al., 2013; Libois et al., 2014, 2015) where it gives realistic predictions of density and snow type profiles (Brun et al., 1992; Vionnet et al., 2012), snow temperature profile (Brun et al., 2011 and snow specific surface area and permeability (Carmagnola et al., 2014; Domine et al., 2013). It has been recently optimized for application to conditions prevailing at Dome C, Antarctica (Libois et al., 2014) to account for specific conditions such as high snow density values at the surface and low precipitation amounts.

The high vertical spatial resolution of Crocus, its interactive simulation of snow metamorphism in near-surface snow and firn makes it a good basis for the study of post-deposition effects in low accumulation regions. For the purpose of this study, we thus implemented vapor transport resulting from temperature gradients and the water isotope dynamics into the Crocus model. This article presents this double implementation, and a series of sensitivity tests. While a perfect match of observations is not anticipated, in part because not all relevant processes are represented in the model, this study represents thus a first step towards better understanding the impact of diffusion driven by temperature gradients on the snow isotopic composition.

2 Physical basis

The isotopic composition of the snow can evolve after deposition due to several processes. Here, we first give a rapid survey of such processes at the macroscopic level (modification of the isotopic composition of a centimetric/decametric snow layer after exchanges with the other layers). Second, we consider the evolution of the isotopic composition at the microscopic level, i.e. at the level of the microstructure. Indeed, the macroscopic change of the isotopic composition results from both large scale and small scale processes. For instance, dry metamorphism includes both vapor transport from one layer to another, and vapor/ice grain exchange inside a layer.

2.1 Evolution of the snow layers composition (macroscopic scale)

Several studies address the evolution of the isotopic compositions in the snow column after deposition. Here, following Ekaykin et al., 2009, we separate random processes that induce smoothing of the original isotope profile (attenuation of amplitude) without modification of the mean local pluriannual value, from oriented processes which affect also the mean local pluriannual value (accumulation of light or heavy isotopes in some layers).

2.1.1 Signal attenuation on a vertical profile (smoothing)

The smoothing of isotopic compositions with conservation of the mean local pluriannual value is caused by diffusion against isotopic gradients in vapor phase and in solid phase. The magnitude of smoothing depends on site temperature, and on accumulation. Indeed, higher temperatures correspond to higher vapor densities, and also higher diffusivities in the vapor and solid phases. Oppositely, high accumulation rates ensure a greater separation between seasonal $\delta^{18}O$ peaks (Ekaykin et al., 2009; Johnsen et al., 1977) thereby limiting the impact of diffusion. Because sites with high accumulation rates also usually have higher temperatures, the resulting effect on diffusion is still unclear. These two competing effects should be thoroughly investigated and Johnsen et al. (2000) displays the damping amplitude of a periodic signal depending on wavelength and on diffusion length, strongly driven by temperature.

In Greenland, Johnsen et al. (1977) indicate that annual cycles generally disappear at sites with accumulation lower than 200 kg m^{-2} yr^{-1}. Diffusion against isotopic gradients exists throughout the entire snow/ice column, but is more intense in the upper layers with larger porosities.

2.1.2 Signal shift caused by oriented processes

We consider here the oriented movement of water molecules forced by external variables such as temperature or pressure. Three processes can contribute to oriented vapor transport and hence possible isotopic modification within the snowpack: diffusion, convection, and ventilation (Albert et al., 2002). Convection is not considered here, since Brun et Touvier (1987) have demonstrated that convection of dry air within the snow as a response to strong temperature gradients cannot occur except in case of very low snow density (~100 kg/m^3) which are generally not encountered in Antarctic snow. Bartelt et al. (2004) also indicate that energy transfer by advection is negligible compared to energy transfer by conduction in the first meters of the snowpack. The two other processes, ventilation and diffusion are forced respectively by variations of the surface pressure and surface temperature. In the first case, the interaction between wind and surface roughness is responsible for wind-pumping, i.e. renewal of the air of the porosity through macroscopic air movement (Albert et al., 2002; Colbeck, 1989, Neumann et al., 2004). In the second case, air temperature diurnal or seasonal variations generate vertical temperature gradients within the snow (Albert and McGilvary, 1992; Colbeck, 1983), and consequently vertical vapor density gradients, responsible for vapor diffusion. These two processes are largely exclusive (Town et al., 2008) because strong ventilation homogeneize the air and vapor in the porosity and therefore prevents diffusion. Diffusion as a result of temperature gradients can coexist with ventilation only at very low air velocities (Calonne et al., 2015). It becomes the main process of vapor transport when air is stagnant in the porosity.

2.2 Evolution of the isotopic composition at the microscopic scale

2.2.1 Conceptual representation of snow microstructure as spherical grains

The term "snow grain" as used classically is an approximation. In reality, 'snow grains' are very diverse in size, shape, degree of metamorphism and may also be made of several snow crystals agglomerated. Moreover, they are often connected to each other, forming an ice matrix ('snow microstructure'). However, several studies addressing snow metamorphism physical processes have relied on spherical ice elements to represent snow grains and snow microstructure (Legagneux and Domine, 2005, Flanner and Zender, 2006). Here, we consider that the snow grains are made of two concentric layers (one internal and one external) with different isotopic compositions. In terms of snow microstructure, this could correspond to inner vs. outer regions of the snow microstructure.

Indeed, the snow grain (or the snow microstructure) is not necessarily homogeneous in terms of isotopic composition. On the one hand, the center of the grain (inner region of the microstructure) is relatively insulated, and becomes more and more insulated as the grain grows (as the structure gets coarser). On the other hand, outer layers are not necessarily formed at the same time as its center (core of the microstructure), or in the same environment (Lu and DePaolo, 2016). They are prone to subsequent sublimation or condensation of water molecules, implying that their composition may change more quickly and more frequently than in the inner layers. Of course, only the bulk δ^{18}O value of the snow grain can be measured by mass spectrometry, but considering the heterogeneity of the grain may be required to get a fine understanding of the processes. In the following, we propose to split the ice grain compartment into two sub-compartments: grain surface and grain center. Thus, the grain surface isotopic composition is allowed to evolve as a result of exchange with vapor in the porosity (sublimation or condensation) and also as a result of exchange with grain center (through solid diffusion, or grain center translation, see below). The grain center composition evolves at the time scale of week/month, as opposed to the grain surface, where the composition changes at the time scale of the vapor diffusion, i.e. over minutes.

2.2.2 Solid diffusion within snow grains

The grain center isotopic composition may change either as a result of crystal growth/sublimation or as a result of solid diffusion within the grain. For solid diffusion, the transfer of molecules from the grain boundary towards the center of the grain is very slow. The diffusivity of water molecules in solid ice (D_{ice} in $m^2 \cdot s^{-1}$) follows Arrhenius law and thus can be expressed as a function of ice temperature (T) (Gkinis et al., 2014; Johnsen et al., 2000; Ramseier, 1967) using Eq. (1):

$$D_{ice} = 9.2 \cdot 10^{-4} \times \exp\left(\frac{-7186}{T}\right) \qquad (1)$$

Note that all symbols are listed in Table 1.

Thus at 230 K, the diffusivity is 2.5 x 10^{-17} $m^2 \cdot s^{-1}$ which leads to a characteristic time for solid diffusion (Δt_{sol}) across a typical ice grain of radius R_{moy}= 0.1 mm (typical snow grain radius values in the first meter at Dome C, Gay et al. 2002) given by Eq. (2):

$$\Delta t_{sol} = \frac{{R_{moy}}^2}{D_{ice}} = 4.03 \times 10^8 \text{ s, or} \sim 13 \text{ years} \qquad (2)$$

Therefore the solid diffusion between the surface of the grain and the inner part of the grain, at the time scales considered in the model (seconds to months) is close to zero. For the summer months at Dome C (*T*=248 K, from Dec. to Jan., Table 2), the characteristic time becomes 15 months, which remains quite large compared to our time scale. At Summit the grain size is typically larger (0.2 to 0.25 mm in wind-blown and wind pack; 0.5 to 2 mm in the depth hoar layer; Albert and Shultz, 2002), and the summer temperature is also higher (*T*=259 K at GRIP from July to Sept., after Shuman et al., 2001), yielding characteristic time of the order of 30 months (for 0.25 mm).

2.2.3 Snow grain recrystallization

During snow metamorphism, the number of snow grains tends to decrease with time, while the snow grain size tends to increase (Colbeck, 1983). Indeed each grain experiences permanent cycles of sublimation/condensation, but the small grains are more likely to disappear completely, and then there is no more nucleus for condensation at the grain initial position. Oppositely, the bigger grains do not disappear and accumulate the vapor released by the smaller ones. Concurrently to this change of grain size, the grain shape also tends to evolve. In conditions of maintained/stable temperature gradient, facets appear at the condensing end of snow grains, while the sublimating end becomes rounded (Colbeck, 1983). In that case, the center of the grain moves toward the warm air region. This migration causes a renewal of the grain center, on a proportion that can be estimated from the apparent grain displacement (Pinzer et al., 2012). Pinzer et al. (2012) use this method to get an estimation of vapor fluxes (since vapor transports water in the porosity from the 'sublimating' end of an ice grain toward the 'condensing' end of another ice grain).

The asymmetric recrystallization of snow grains implies that the surface layer of the snow grain is eroded at one end and buried at the other end. Therefore, the composition of the grain center changes more often than if the surface layer was thickening (through condensation) or thinning (through sublimation) homogeneously over the grain surface. This means in particular that the 'inner core' of the grain gets exposed more often. Implementing this process is thus very important to have a real-time evolution of the snow grain center isotopic composition. Here, we reverse the method of Pinzer et al. (2012) and use the fluxes of isotopes in vapor phase computed by the model to assess the renewal of the grain center (Sect. 3.1.3.).

3 Material and Methods

3.1 Description of the model (SURFEX/Crocus revision 4805)

We first present the model structure and second describe the new module of vapor transport (diffusion forced by temperature gradients). Third, we present the integration of water isotopes in the new version of the model including the vapor transport module.

3.1.1 Model structure

The Crocus model is a one-dimensional detailed snowpack model, consisting of a series of snow layers with variable and evolving thicknesses. Each layer is characterized by its density, heat content, and by parameters describing snow microstructure (sphericity and specific surface area) (Vionnet et al., 2012, Carmagnola et al., 2014). In the model, the profile of temperature evolves with time as a function of the surface temperature and of the energy fluxes at the surface and at the bottom interface (ice or soil). To correctly compute energy balance, the model integrates albedo calculation, deduced from surface microstructure and impurity content (Brun et al., 1992, Vionnet et al., 2012).

The successive components of the Crocus model have been described by Vionnet et al. (2012). In this subsection, we only list them in order to point out those that we modified to include water stable isotopes and water vapor transfer. Our modifications are described in greater detail in the next sub-sections. Note that the Crocus model has a typical internal time step of 900 s (15 min), corresponding to the update frequency of layers properties. We only refer here to processes occurring in dry snow.

1) Snow fall: The presence/absence of precipitation at a given time is determined from the atmospheric forcing inputs. When there is precipitation, a new layer of snow may be formed (its thickness is deduced from the precipitation amount). This module was modified to include water isotopes (see Sect. 3.1.3).

2) Update of snow layering: At each step, the model may split one layer into two or merge two layers together to get closer to a target vertical profile for optimal calculations (high resolution in the first layers to correctly simulate heat and matter exchanges). The layers that are merged together are the closest in terms of microstructure variables (shape, size). This module was slightly modified to include water isotopes (the new isotopic composition after layer merging is the weighted average of the isotopic compositions of the initial layers).

3) Metamorphism: The microstructure variables evolution follows empirical laws. These laws describe the change of grain parameters as a function of temperature, temperature gradient, snow density and liquid water content. This module was not modified.

4) Snow compaction: The original compaction scheme in Crocus describes the increase of density and the decrease in the layer thickness under the burden of the overlying layers and resulting from metamorphism. Snow viscosity is parameterized using the layer density and also using information on the presence of hoar or liquid water. However this parameterization of the viscosity was designed for alpine snowpack (Vionnet et al., 2012) and may not be adapted to polar snow packs. Here, we used a simplified compaction scheme, where the compaction rate is constant with time and taken to compensate yearly accumulation (Eq. (3), see Sect. 3.3. for accumulation rates).

$$\frac{1}{\rho_{sn}(t,n)} \times \frac{\rho_{sn}(t+dt,n)-\rho_{sn}(t,n)}{dt} = \frac{1}{m_{sn}(t,n)} \times \frac{dm_{sn}}{dt} \tag{3}$$

Note that symbols ρ_{sn}, m_{sn} and t are defined in Table 1.

5) Wind drift events: They modify the properties of the snow grains which tend to become more rounded, and also increase the density of the first layers through compaction (higher degree of packing of the grains). An option allows snow to be partially sublimated during these wind drift events (Vionnet et al., 2012). This module was not modified.

6) Snow albedo and transmission of solar radiation: for each layer, snow albedo and absorption coefficient are computed from snow microstructure properties and impurity content (computed based on snow age) in three wavelength bands, using the properties of the two uppermost snow layers. Incoming solar radiation is partly reflected (using albedo value), the rest of the radiation penetrates into the snowpack. Then, for each layer starting from the top, incoming radiation is partly absorbed (using absorption coefficient) and partly transmitted to the layer underneath. This module was not modified.

7) Latent and sensible surface energy and mass fluxes: The sensible heat flux and the latent heat flux are computed using the aerodynamic resistance and the turbulent exchange coefficients. This module was not modified.

8) Vertical snow temperature profile: It is deduced from the heat diffusion equation, using the snow conductivity, as well as the energy balance at the top (radiation, latent heat, sensible heat) and at the bottom of the snowpack. This module was not modified.

9) Snow sublimation and condensation at the surface: The amount of snow sublimated/condensed is deduced from the latent heat flux, and the thickness of the first layer is updated. Other properties of the first layer (density, SSA) are kept constant. This module was not modified.

3.1.2 Implementation of water transfer

We developed a new vapor transport subroutine which has been inserted after the compaction (4) and wind drift (5) modules, and before the solar radiation module (6). The flux of vapor at the interface between two layers is obtained using the Fick's law of diffusion (Eq. (4)):

$$F(n+1 \rightarrow n) = \frac{-2\, D_{eff}(t,n \rightarrow n+1)(\rho_v(t,n) - \rho_v(t,n+1))}{dz(t,n) + dz(t,n+1)} \quad (4)$$

where $dz(t, \mathrm{n})$ and $dz(t, n+1)$ are the thicknesses of the two layers considered in meters, $\rho_v(t, n)$ and $\rho_v(t, n+1)$ are the local vapor densities in the two layers (kg m^{-3}), and $D_{eff}(t, n \rightarrow n+1)$ (m^2 s^{-1}) is the effective diffusivity of water vapor in the snow at the interface. The thicknesses are known from the previous steps of the Crocus model and account for snowfall and snow layering modifications, but the vapor densities and the interfacial diffusivities must be computed.

The effective diffusivity at the interface is obtained in two steps: first the effective diffusivities ($D_{eff}(t,n)$ and $D_{eff}(t,n+1)$) in each layer are calculated (Eq. (5)), second, the interfacial diffusivity is computed as their harmonic mean (Eq. (6)). Effective diffusivity can be expressed as a function of the snow density using the relationship proposed by Calonne et al. (2014), for layers with relatively low density compacting mostly by boundary sliding (grains slide on each other but do not interpenetrate). It is the case for our study where density is always below 600 kg m^{-3}. The equation of Calonne et al. (2014) is based on the numerical analysis of 3D tomographic images of different types of snow. It relates normalized effective diffusivity (D_{eff} / D_v, where D_v is the vapor diffusivity in air and has a value of $2.036 \cdot 10^{-5}$ m^{2}s^{-1}, Calonne et al., 2014) to the snow density (ρ_{sn}) in the layer. ρ_i corresponds to the density of ice (917 kg m^{-3}). Here we do not take into account the effect of temperature on D_v.

$$\frac{D_{eff}(t,n)}{D_v} = \frac{3}{2}\left(1 - \frac{\rho_{sn}(t,n)}{\rho_{ice}}\right) - \frac{1}{2} \quad (5)$$

$$D_{eff}(t, n \rightarrow n+1) = \frac{1}{\frac{1}{D_{eff}(t,n)} + \frac{1}{D_{eff}(t,n+1)}} \quad (6)$$

We assume that vapor is in general at saturation in the snow layers (Neumann et al., 2008; Neumann et al., 2009). The local vapor density ρ_v (kg m^{-3}) in each layer is given by the Clausius-Clapeyron equation (Eq. (7)):

$$\rho_v(t,n) = \rho_{v0}\exp\left(\frac{L_{sub}}{R_v \rho_{ice}}\left(\frac{1}{T_0} - \frac{1}{T(t,n)}\right)\right) \quad (7)$$

where, ρ_{v0} is the vapor density at 273.16 K (2.173 10^{-3} kgm^{-3}), L_{sub} is the latent heat of sublimation (2.6 10^{9} Jm^{-3}), R_v is the vapor constant (462 Jkg^{-1}K^{-1}), ρ_{ice} is the density of ice (917 kgm^{-3}), T_0 is the temperature of the triple point of water (273.16 K) and T is the temperature of the layer.

All layers are treated identically, except the first layer at the top and the last layer at the bottom. For the uppermost layer, the exchange of vapor occurs only at the bottom boundary since exchanges with the atmosphere are described elsewhere in Crocus (step 9, surface energy balance). For the lowermost layer, only exchanges taking place at the top boundary are considered, the flux of vapor to/from the underlying medium being set to zero.

For each layer, vapor density and effective diffusivity are computed within the layer and in the neighboring layers. Fluxes at the top and bottom of each layer are deduced from Fick's law of diffusion (Eq. 4). They are integrated over the subroutine time step (1 s), and the new mass of the layer is computed and used at the beginning of the next subroutine step. The choice of a small time step within the subroutine (the time step in the main routine is 900 s) ensures that vapor fluxes remain small relative to the amount of vapor present in the layers. Note that the temperature profile, which controls the vapor density profile, is not modified within the subroutine. Physically, temperature values should change as a result of the transfer of sensible heat from one layer to another associated with vapor transport, as well as due to the loss or gain of heat caused by water sublimation or condensation, respectively, in warm or cold layers, respectively (Albert and McGilvary, 1992; Kaempfer et al., 2005). However, vapor transport is only a small component to heat transfer between layers (Albert and Hardy, 1995; Albert and McGilvary, 1992). With or without vapor diffusion, the steady-state profile for temperature varies by less than 2% (without ventilation) (Calonne et al., 2014). Thus the effect can be neglected at first order.

3.1.3 Implementation of water isotopes

To enable the Crocus model for isotopes, 1) we introduce a new variable for isotopes, and 2) we compute its value in snowfall, as well as 3) its evolution with time, as a result of layer merging or diffusion. The isotopic composition of snow in each layer is represented by the triplicate (δ^{18}O, d-excess, ^{17}O-excess). Only the results of δ^{18}O are presented and discussed here. Moreover, for each parameter, two values per layer are considered independently, corresponding to the 'snow grain center' and the 'snow grain surface', respectively. Water vapor isotopic composition is deduced at each step from the 'snow grain surface' isotopic composition, and not stored independently (to limit the number of prognostic variables). To compute the evolution of isotopic compositions, we modified the Crocus model at step 1 (snowfall), and after step 5 (within the new module of vapor transfer described in Section 3.1.2.).

In the snow fall subroutine, a new layer of snow may be added (depending on the weather) at the top of the snowpack. At this step of the routine, we suppose that the snow grains that are deposited are homogenous (same composition in the "grain surface" compartment and in the "grain center" compartment). We deduce their isotopic composition from the air temperature (see Sect. 3.2.).

Within the new vapor transport subroutine, we add a specific module that modifies the isotopic compositions in the two snow grain sub-compartments as a result of water vapor transport and recrystallization of snow crystals. It works with four main steps:

1) an initiation step where the vapor isotopic compositions are computed, using equilibrium fractionation, from the ones in the grain surface sub-compartment,

2) a transport step where vapor moves from one layer to another, with kinetic fractionation associated with diffusion,

3) a balance step where the new vapor in the porosity exchanges with the grain surface compartment (sublimation/condensation) with a flux determined by the difference between actual vapor density and expected vapor density at saturation,

and 4) a 'recrystallization' step where the grain center and grain surface isotopic compositions are homogenized, leading to an evolution of grain center isotopic composition.

The time step in this module is 1s, the same as the time step of the sub-routine.

The initial vapor isotope composition $R^*_{vap\ ini}$ in a given layer is taken at equilibrium with the 'grain surface' isotopic composition $R^*_{surf\ ini}$. Here * denotes heavy isotope, and thus stands for ^{18}O, ^{17}O or D. Equilibrium fractionation is a hypothesis that is correct in layers where the air has been standing still for a long time in the porosity and where vapor has reached equilibrium with ice grains, physically and chemically. To compute isotopic ratios for water vapor we use the following Eq. (8) and (9):

$$\begin{cases} R^{18}_{vap\ ini} = \alpha^{18}_{sub} \times R^{18}_{surf\ ini} \\ R^{17}_{vap\ ini} = \alpha^{17}_{sub} \times R^{17}_{surf\ ini} \\ R^{18}_{vap\ ini} + R^{17}_{vap\ ini} + 1 = 1/c^{16}_{vap\ ini} \end{cases} \tag{8}$$

$$\begin{cases} R^{D}_{vap\ ini} = \alpha^{D}_{sub} \times R^{D}_{surf\ ini} \\ R^{D}_{vap\ ini} + 1 = 1/c^{1H}_{vap\ ini} \end{cases} \tag{9}$$

The equilibrium fractionation coefficients ($\alpha_{sub}{}^*$) are obtained using the temperature-based parameterization from Ellehoj et al. (2013).

The initial vapor density $\rho_{vap\ ini}$ has already been computed in the vapor transport subroutine, and the volume of the porosity can be obtained from the snow density (ρ_{sn}) and the thickness of the layer (*dz*). By combining both, we obtain Eq. (10) which gives the initial mass of vapor in the layer ($m_{vap\ ini}$).

$$m_{vap\ ini} = \rho_{vap\ ini} \times \left(1 - \frac{\rho_{sn}}{\rho_{ice}}\right) \times dz \tag{10}$$

This mass of vapor should be subtracted from the initial grain surface mass (as vapor mass is not tracked outside of the sub-routine, see Fig. 1) so that the new grain surface isotope composition, after vapor individualization is given by Eq. (11):

$$c^{18}_{surf\ new} = \frac{m^{18}_{surf\ new}}{m_{surf\ new}} = \frac{m^{18}_{surf\ ini} - m_{vap\ ini} \times c^{18}_{vap\ ini}}{m_{surf\ ini} - m_{vap\ ini}} \tag{11}$$

Refer to Table 1 for the definition of symbols.

The diffusion of isotopes follows the same scheme as the water vapor diffusion described above in Sect. 3.1.2. and Eq. (4). In Eq. (12), the gradient of vapor density is replaced by a gradient of concentration of the studied isotopologue. The kinetic fractionation is realized with the *D*/D* term (where * stands for ^{18}O or ^{17}O or ^{2}H; Barkan and Luz, 2007).

$$F^{18}(n+1 \rightarrow n) = \frac{-2 \times D_{eff,n\&n+1}\left(\rho_v(t,n) \times c^{18}_{vap\ ini}(t,n) - \rho_v(t,n+1) \times c^{18}_{vap\ ini}(t,n+1)\right)}{dz(t,n) + dz(t,n+1)} \times \frac{D^{18}}{D} \tag{12}$$

Refer to Table 1 for symbol definitions.

As done for water molecules transport (Sect. 3.1.2.), the flux is set to zero at the top of the first layer and at the bottom of the last layer. Note that when the total flux of vapor is null (same vapor density in the two adjacent layers), we still have isotopic diffusion because of the isotopic concentration gradients (Eq. (12)). In that case, heavy and light molecules cross the boundary in opposite directions, with a null absolute flux of water molecules across the boundary. Once top and bottom fluxes of each layer have been computed, the new masses of the various isotopes in the vapor are deduced, as well as the new ratios.

After the exchanges, the isotopic composition in the vapor has changed. However, because the vapor isotopic composition is not a prognostic variable outside of the vapor transport subroutine, this change must be transferred to either the 'grain surface compartment' or to the 'grain center compartment' before leaving the subroutine. First, we consider exchanges of isotopes with the grain surface compartment, which is in direct contact with the vapor. Depending on the net mass balance of the layer, two situations must be considered:

1) If the mass balance is positive, the transfer of isotopes takes place from the vapor toward the grain surface (condensation). To evaluate the change in the isotope composition in the grain surface, the mass of vapor condensed ($\Delta m_{vap,exc}$) must be computed. It is the difference between the mass of vapor expected at saturation (note that temperature does not evolve in this subroutine), and the mass of vapor present in the porosity after vapor transport. This difference is not exactly equal to the mass of vapor that has entered the layer, as a consequence of layer porosity change. The excess mass of vapor is given by Eq. (13):

$$\Delta m_{vap,exc} = \left[(\rho_{sn\,new} - \rho_{sn\,ini}) + \rho_v \times \left[\left(1 - \frac{\rho_{sn\,ini}}{\rho_{ice}}\right) - \left(1 - \frac{\rho_{sn\,new}}{\rho_{ice}}\right)\right]\right] \times dz \tag{13}$$

Refer to Table 1 for the list of symbols.

Since the excess of vapor is positive, the next step is the condensation of the excess vapor. Here the condensation of excess vapor occurs without additional fractionation. The number of excess water molecules is determined through comparison with the expected number in the water vapor phase for equilibrium state between surface snow and water vapor. They are drawn to cold grains and get stuck.

2) If the mass balance is negative, the transfer of isotopes takes place from the grain surface toward the vapor without fractionation. Ice from the grain surface sub-compartment is sublimated without fractionation to reach the expected vapor

density. Note that the absence of fractionation at sublimation is a frequent hypothesis, because water molecules move very slowly in ice lattice (Friedman et al., 1991; Neumann et al., 2005; Ramseier, 1967), and thus the sublimation removes all the water molecules present at the surface of grains, including the heaviest ones before accessing inner levels. Note that in reality, there are evidences for fractionation at sublimation, either through kinetic effects associated with sublimation / simultaneous condensation or equilibrium fractionation at the boundary, especially when invoking the existence of a thin liquid layer at the snow – air interface (Neumann et al., 2008 and references therein; Sokratov and Golubev, 2009; Stichler et al., 2001; Ritter et al., 2016). The new composition in the vapor results from a mixing between the vapor present and the new vapor recently produced. The composition in the 'grain surface' ice compartment does not change.

The limit between the surface compartment and the grain center compartment is defined by the mass ratio of the grain surface compartment to the total grain mass ($\tau=m_{surf}/(m_{center}+ m_{surf})$, Fig. 1, symbols listed in Table 1). This mass ratio can be used to determine the thickness of the 'grain surface layer' as a fraction of grain radius, for spherical grains. The surface compartment must be thin, to be able to react to very small changes in mass when vapor is sublimated or condensed. Because of the numerical precision of our model (6 decimals) run at a 1 s temporal resolution, the isotopic composition of the surface compartment can change in response to surface fluxes only if its mass is smaller than 10^6 the mass of the water vapor present in the porosity ($m_{surf}<10^6 m_{vap}$, or $m_{surf} /(m_{center}+ m_{surf})$, $<10^6 \frac{\Phi \rho_v V_{tot}}{\rho_{sn} V_{tot}}$, i.e. $\tau< \frac{\rho_v \Phi}{\rho_{sn}} 10^6$). Here V_{tot} corresponds to the total volume of the layer whereas Φ represents its porosity. On the other hand, this compartment must be thick enough to transmit the change in isotopic compositions caused by vapor transport and condensation/sublimation to the grain center. Again, numerical precision imposes that its mass should be no less than 10^{-6} times the mass of the grain center compartment ($\tau>10^{-6}$). Considering typical temperatures, snow densities and layer thicknesses (Table 3) such approach leads to a range for the ratio τ between 10^{-6} (minimum value to influence the grain center) to $1.3\cdot10^{-3}$ (maximum value to perceive the influence of exchanges with water vapor). Here we use a ratio $\tau=5\cdot10^{-4}$ for the mass of the grain surface relative to the total mass of the layer (Fig. 1). We have run sensitivity tests with smaller and larger ratios (Sect. 4.1.4.).

Here, we implement two types of mixing between grain surface and grain center in the model. The first one is associated with crystal growth or shrinkage, as a result of vapor transfer. Mixing is performed at the end of the vapor transfer subroutine, after sublimation/condensation has occurred. During the exchange of water between vapor and grain surface, the excess (or default) of mass in the water vapor caused by vapor transport has been entirely transferred to the grain surface sub-compartment. Thus the mass ratio between the grain surface compartment and the grain center compartment deviates from the original one. To bring the ratio back to normal (τ=5·10^{-4}) mass is transferred either from the grain surface to the grain center or from the grain center to the grain surface. This happens without fractionation, i.e. if the transfer occurs from the center to the surface, the composition of the center remains constant.

The second type of mixing implemented is the grain center translation (Pinzer et al., 2012) which favors mixing between grain center and grain surface in the case of sustained temperature gradient. While Pinzer et al. (2012) used the apparent grain displacement to compute vapor fluxes, here we reverse this method and use the vapor fluxes computed from Fick's law to estimate the grain center renewal. However, instead of transferring a small proportion of the surface compartment to the grain center every second, we choose to transfer the totality of the snow grain surface compartment every few days (total mixing of the grain). The interval $\Delta t_{surf/center}$ between two successive mixings is derived from the vapor flux F(n+1→n) within the layer using Eq. (14).

$$\boldsymbol{\Delta t_{surf/center}} = \frac{\boldsymbol{m_{sn} \times \tau}}{\boldsymbol{F(n+1 \rightarrow n)}} \tag{14}$$

Using a typical flux $F(n+1 \rightarrow n)$ of 1.3 10^{-9} kg·m^{-2}·s^{-1} (for the average temperature gradient of 3 °C m^{-1}) and a typical mass for the layer of m_{sn} of 3.3 kg (i.e. a mass for the grain surface compartment of m_{sn} τ), the dilution of the grain surface compartment into the grain center should occur every 15 days. Of course, this is only an average, since layers have varying masses, and since the temperature gradient can be larger or smaller. We will however apply this time constant for all the layers and any temperature gradient (see sensitivity tests Sect. 4.1.4.), because it is necessary that the mixing between compartments occur at the same time in all layers.

In terms of magnitude, this process is probably much more efficient for mixing between the two sub-compartments of the solid grain than grain growth or solid diffusion. It is thus crucial for the modification of the bulk isotopic composition of the snow layer. It makes the link between microscopic processes and macroscopic results.

3.1.4 Model initialization

For model initialization, an initial snowpack is defined, with a fixed number of snow layers, and for each snow layer an initial value of thickness, density, temperature and $\delta^{18}O$. Typically, oriented processes such as diffusion and ventilation occur mainly in the first meters of snow so that the model starts with an initial snowpack of about 12 m.

The choice of the layer thicknesses depends on the annual accumulation. Because the accumulation is much higher at GRIP than at Dome C (Sect. 3.2., Table 2), the second site is used to define the layer thicknesses. About 8 cm of fresh snow are deposited every year (Genthon et al., 2016; Picard et al., 2016; Libois et al., 2014), which implies that in order to keep seasonal information, at least one point every 4 cm is required in the first meter. We impose maximal thickness of 2 cm for the layers between 0 and 70 cm depth and a maximal thickness of 4 cm for the layers between 70 cm and 2 meters depth. Below 2 meters, the thicknesses are set to 40 cm or even 80 cm. Thus the diffusion process can only be studied in the first 2 m of the model snowpack. In the very first centimeters of the snowpack, thin layers (mm) are used to accommodate low precipitation amounts, and surface energy balance (radiations…). The initial density profiles are defined for each site specifically (see Sect. 3.2.). The initial temperature and $\delta^{18}O$ profiles in the snowpack depend on the simulation considered (see Sect. 3.3.).

3.1.5 Model output

A data file containing the spatio-temporal evolution of prognostic variables such as temperature, density, SSA or $\delta^{18}O$ is produced for each simulation. Here, we present the results for each variable as two dimensional graphs, with the time on the horizontal axis and the snow height as the vertical axis. The variations of the considered variable are displayed as color levels. As indicated above, only the first 12 m of the polar snowpack are included in the model. The bottom of this initial snowpack constitutes the vertical reference (zero) to measure vertical heights (h). The height of the top of the snowpack varies with time due to snow accumulation and to snow compaction. In the text, we sometimes refer to the layer depth (z) instead of its height (h). The depth z can be computed at any time by subtracting the current height of the considered layer from the current height of the top of the snowpack.

3.2. Studied sites: meteorology and snowpack description

In this study we run the model under conditions encountered at Dome C, Antarctica and GRIP, Greenland. We chose these two sites because they have been well-studied in the recent years through field campaigns and numerical experiments. In particular, for Dome C, a large amount of meteorological and isotopic data is available (Casado et al., 2016a; Stenni et al., 2016; Touzeau et al., 2016). Typical values of the main climatic parameters for the two studied sites (Summit and Dome C) are given in Table 2, as well as typical δ^{18}O range. Dome C has lower accumulation rates (2.7 cm i.e., Table 2) than Summit (23 cm i.e./yr, Table 2), making it more susceptible to be affected by post-deposition processes.

The δ^{18}O value in the precipitation at a given site reflects the entire history of the air mass, including evaporation, transport, distillation, and possible changes in trajectory and sources. However, assuming that these processes are more or less repeatable from one year to the next, it is possible to empirically relate the δ^{18}O to the local temperature, using measurements from collected samples. Here, using data from one year snowfall sampling at Dome C (Stenni et al., 2016; Touzeau et al., 2016), we use the following Eq. (15) to link $\delta^{18}O_{sf}$ in the snowfall to the local temperature ($\boldsymbol{T_{air}}$, in K):

$$\delta^{18}O_{sf} = 0.45 \times (T_{air} - 273.15) - 31.5 \quad (15)$$

The density profile in the snowpack is obtained from fitting density measurements from Greenland and Antarctica (Bréant et al., 2016). Over the first 12 m of snow, we obtain the following evolution (Eq. (16) and Eq. (17)) for NGRIP (in the absence of density measurements at GRIP) and Dome C respectively:

$$\rho_{sn}(t,n) = 17.2 \cdot z(t,n) + 310.3 \quad \text{(N=22; R}^2\text{=0.95)} \quad (16)$$

$$\rho_{sn}(t,n) = 12.41 \times z(t,n) + 311.28 \quad \text{(N=293; R}^2\text{=0.50)} \quad (17)$$

3.3 List of simulations

3.3.1 Greenland simulation

The first simulation (number 1 in Table 4) is dedicated to the study of diffusion against isotopic gradients, and is realized on a Greenland snowpack with an initial sinusoidal profile of δ^{18}O (see Eq. 18) and a uniform and constant vertical temperature profile at 241 K. In addition to comparison to δ^{18}O profiles for GRIP and other Greenland sites, the aim of the first simulation is to compare results from Crocus model to the models of Johnsen et al. (2000) and Bolzan and Pohjola (2000) run at this site with only diffusion against isotopic profiles. To compare our results to theirs, we consider an isothermal snowpack, without meteorological forcing, and we deactivate modules of surface exchanges and heat transfer. The initial seasonal sinusoidal profile at GRIP is set using Eq. (18):

$$\delta^{18}O(t,n) = -35.5 - 8 \times \sin\left(\frac{2\pi \times z(t,n)}{a \times \rho_{ice}/\rho_{sn}(t,n)}\right) \quad (18)$$

where z is the depth of the layer n, $\rho_{sn}$is its density, ρ_{ice} is the density of ice (917 kg m^{-3}), a is the average accumulation at GRIP (a=0.23 m i.e./yr, Guillevic et al., 2013). The amplitude value of 16 ‰ is close to the back-diffused amplitude at Summit (Sjolte et al., 2011).

The second simulation is run with evolving temperature in the snowpack (computed by the model, using meteorological forcing from ERA-Interim, see Table 4). In that case, isotopic diffusion in the vapor phase results both from diffusion against isotopic gradients and from vapor density gradients. The initial snowpack is the same as in the previous simulation.

In the two GRIP simulations, the modules of wind compaction and weight compaction are inactive. Indeed, as weight compaction is taken to compensate yearly accumulation (Eq. (3)), applying this compaction in a case without precipitation would lead to an unrealistic drop in snow level. The wind compaction was absent from the model of Johnsen et al. (2000) and using this module would make comparisons more difficult.

3.3.2 Dome C simulations

We take advantage of the high documentation of the Dome C site to disentangle the different effects on the variations of snow density and water isotopic composition, hence with a high number of simulations (4). The simulations at Dome C were performed with an evolving temperature profile (simulations 3 to 6). We use modified meteorological forcing from ERA-Interim (Dee et al., 2011; Libois et al., 2014; see details in Table 4), and the modules of energy exchange and transfer within the snow to compute temperatures in the snow layers. In this series of simulations, the densities and $\delta^{18}O$ values thus evolve as a result of diverging and/or alternating vapor fluxes. The simulations are ordered by increasing complexity. First, the modules of homogeneous compaction and wind drift are deactivated, as well as the module of snowfall (Simulation 3). Thus the impact of vapor transport forced by temperature gradients on the snow densities is clearly visible. Then the module of compaction and the module of wind drift are activated, to see their impact on the snow density and isotopes (Simulation 4). We use an accumulation rate for Dome C of 0.001 kg m^{-2} per 15 min (dm_{sn}/dt in Eq. (3)). Next snowfall is added, to assess how new layers affect both snow density and snow $\delta^{18}O$ values (Simulation 5). Lastly we run a simulation (6) over 10 years at Dome C, in order to build up a snowpack with realistic 'sinusoidal' variation in $\delta^{18}O$ values.

3.3.3 Summary of the simulations

Table 4 presents the model configuration for the 6 simulations considered here.

4 Results

4.1 Greenland

4.1.1 Results of the Crocus simulations

Figure 2 shows the result of the first simulation, where only diffusion against isotopic gradients is active, as in Johnsen et al., 2000. As expected the maxima and minima of the grain center isotopic composition ($\delta^{18}O_{gcenter}$) are reduced as a result of diffusion. Over 10 years (2000-2009), the amplitude decreases by -1.3 ‰ which corresponds to 8 % variation.

Figure 3 shows the result of the second simulation, i.e. with varying temperature in the snowpack. The results are very similar to the results from the first simulation, except in the first 2-3 cm, which show a greater depletion over the period (-1.8 ‰ instead of -0.5 ‰). This depletion probably results from arrival of ^{18}O-depleted water vapor from warmer layers below. The vapor transport here is forced by the temperature gradients which were absent from the previous simulation. However, several processes are neglected here (precipitation, exchange of vapor with the atmosphere) that could counteract this effect in natural conditions and we thus do not focus more on this first layer. In the layers below (first meter of snow) the half-attenuation is of 0.76 ‰, corresponding to an attenuation of 1.6 ‰, and to a relative attenuation of 9.5 % of the initial amplitude. This result is very similar to the one obtained in the first, simplified simulation. In conclusion, at GRIP, the diffusion of vapor as a result of temperature gradients has only a limited impact on isotopic compositions, and most of the simulated attenuation can be attributed to diffusion against isotopic gradients.

4.1.2 Comparison with core data

Here we evaluate the attenuation of the initial seasonal signal in $\delta^{18}O$ over 10 years at NEEM using 4 shallow cores (NEEM2010S2, NEEM2008S3, NEEM2007S3, NEEM2008S2) published in Steen-Larsen et al., 2011 and in Masson-

Delmotte et al., 2015, and at GRIP using one shallow core (1989-S1), published in White et al., 1997. For NEEM the values of the four cores are taken together. For NEEM and GRIP, the half-amplitude is computed along the core, and the maximum value every 20 cm is retained (Fig. 4). Maximum half-amplitudes every 5 m are also computed. The 2.5 m attenuation is greater at GRIP (86 %) than at NEEM (90 %, Fig. 4): the amplitude decreases with depth in parallel for the two cores, with the amplitude at NEEM staying always higher than at GRIP. For comparison with our model, we estimate attenuation after 10 years (~5.8 m deep at NEEM and ~5.65 m deep at GRIP); the remaining amplitude is 80 % and 72 % at GRIP and NEEM respectively. Our simulation produced 8 % of attenuation only on the same duration, showing that our model (run on an isothermal snowpack) underestimates the attenuation observed in the data.

4.1.3 Comparison with other models

At 2.5 m at NGRIP, Johnsen et al. (2000) simulate remaining amplitude of 77 % (Fig. 4). For a depth of 5.43 m, corresponding to an age of 10 years, the remaining amplitude is 57 %. For Bolzan and Pohjola, at GRIP after 10 years (1977-1987) 70 % of the initial amplitude is still preserved. The slower attenuation for Bolzan and Pohjola (2000) compared to Johnsen et al. (2000) may be due more to the different sites (NGRIP/GRIP) than to the different models. Indeed, GRIP has higher accumulation rates that should limit diffusion. Nevertheless, the attenuation simulated by Bolzan and Pohjola at GRIP is stronger than the one simulated in our model (30 % vs 8 %). Town et al. (2008, Sect. [31]) found attenuations of a few tenth of per mil after several years when implementing only diffusion, a result consistent with ours (-1.3 ‰ after 10 years).

We explore below the reasons for discrepancies between models. The equation for effective diffusivity of vapor in firn used in our study is different from the one used by Johnsen et al. (2000) and from the one used by Bolzan and Pohjola (2000). Contrary to the previous authors we do not consider the impact of temperature on the diffusivity in air (D_v) and we do not take into account the tortuosity factor (l), nor the adjustable scale factor (s) of Bolzan and Pohjola. However, using the values given by the previous authors for l and s lead to D_{eff} values ranging from 6.7 10^{-6} to 9.9 10^{-6} m^2s^{-1} for a density of 350 kgm^{-3} and a temperature of 241 K which is coherent with our value of 8.7 10^{-6} m^2s^{-1}. As indicated by Bolzan and Pohjola, the choice of one equation or another has little impact here.

The most probable difference lie in the way diffusion is taken into account. Johnsen et al. (2000) and Bolzan and Pohjola (2000) use a single equation of diffusion to predict the evolution of the isotopic composition of the layer while we specifically compute the fluxes in the vapor, as a result of isotopic gradients, and deduce the evolution of $\delta^{18}O$ in the grain center, after sublimation/condensation and recrystallization. Denux (1996) and van der Wel et al. (2015) indicate that the model by Johnsen et al. (2000) overestimates the attenuation compared to observed values. For Denux (1996), the model by Johnsen et al. (2000) should take into account the presence of ice crusts and the temperature gradients in the surface snow to get closer to the real attenuation at remote Antarctic sites. For van der Wel et al. (2015), the discrepancy between Johnsen et al.'s model prediction and actual measured attenuation at GRIP could have three causes: ice crusts, a bad knowledge and parametrization of the tortuosity in the first meters of snow, and/or a bad description of the isotopic heterogeneity within the ice grain. In our model, the grain heterogeneity is included. Even if the parameters defining the mixing between the two compartments are not very well constrained (see Sect. 4.3.), the attenuation is indeed smaller compared to Johnsen et al.'s model.

4.2 Dome C (Antarctica)

4.2.1 Simulation without precipitation, without wind drift, and without homogeneous compaction

The aim of the following simulations is to isolate diffusion, from other effects affecting snow density as well as water isotopic composition, i.e. wind-drift and compaction.

When only taking into account temperature profiles variations in the firn, the maximum density change occurs in the first layers with an increase of +112 kg m^{-3} over one year (Fig. 5). The additional water comes most probably from the underlying layers which show a progressive decrease in density of -20.5 kg m^{-3} over one year. This upward flux of vapor in the top millimeters of snow reflects a slightly colder temperature at the top of the snowpack, and this even in summer, due to infrared radiation.

Density changes are very limited during winter. As long as the atmosphere remains cold, vapor moves upward, but in very small quantities, insufficient to make the summer density increase disappear. During short warm events in winter (in particular on the 1st of August) the first layer loses mass, but again the change remains small compared to the change observed in summer. As a conclusion, it seems that temperatures above about 240 K are required to observe a significant change in densities at the seasonal scale.

As observed for the density, the main changes of isotopic compositions in the grain surface ($\delta^{18}O_{gsurf}$) and grain center ($\delta^{18}O_{gcenter}$) compartments occur in summer (Fig. 6). During these periods, the first 20 cm of snow tend to become ^{18}O-enriched (+0.2 ‰), due to vapor departure. However, the first 1-2 cm become depleted (-1.1 ‰) because of the condensation of water vapor. During winter, the dispersion of $\delta^{18}O_{gcenter}$ values is only slightly reduced.

Warm events during winter (1st of August, for instance) cause an increase of δ^{18}O values at the surface, which is particularly visible for the $\delta^{18}O_{gsurf}$ values. Thus it seems that warm events leave an imprint on $\delta^{18}O_{gsurf}$ values in surface snow, through vapor transport, even in the absence of precipitation or condensation from the atmosphere. This mechanism could explain the parallel evolution of surface snow isotopic composition and temperature described by Steen-Larsen et al. (2014) and Touzeau et al. (2016) between precipitation events.

4.2.2 Simulation without precipitation, with wind drift, and with homogeneous compaction

In this simulation, there are three potential sources of density changes: homogeneous snow compaction, wind-induced snow compaction and vapor transport.

Figure 7 shows the total density change over one year. The total density change reaches +115 kg m^{-3} in the first layer. Several events of compaction by wind drift are visible, in particular on the 2nd-3rd of February, the 11th-12th of April, the 23rd-24th of May and on the 3rd-4th of June, on the 18th of October and the 27th of November (see also Fig. S1, density changes per 12 h period). Wind drift events are rare but lead to density changes up to 5 kg m^{-3} per 12 h, while vapor transport occurs every day in summer but never leads to changes larger than 250 g m^{-3} per 12 h. Homogeneous compaction leads to a small density increase of about 3 gm^{-3} per 12 h.

Compaction and wind drift are not supposed to modify directly the δ^{18}O values; however, the change in densities and layer thicknesses modifies slightly the temperature profile and the diffusivities and could have an indirect impact on δ^{18}O values. Figure 8 shows $\delta^{18}O_{gcenter}$ changes that are reduced compared to the simulation without wind drift and compaction. This is coherent with a decrease in the density changes associated with vapor transport in the case with compaction (see Fig. S2).

4.2.3 Simulation with precipitation, with wind drift, with homogeneous compaction

In this simulation, we add precipitation to wind and weight compaction effects. Both snowfall and wind compaction are responsible for irregular changes (resp. positive and negative) of the height of the snowpack (Fig. 9). In terms of density, the new snow deposited has a small density (304 kg m^{-3}), and therefore snowfall tends to decrease the density in the first layer, relative to the original vertical density profile (Fig. 9, Fig. S3a). The effect of snowfall is therefore opposite to the one of wind drift and compaction. As a result of these various processes the density in the first layer varies between 304 and 370 kgm^{-3}.

When δ^{18}O in the precipitation varies with a seasonal cycle, $\delta^{18}O_{gcenter}$ in the new layers varies as expected from -40 ‰ (31th of December) to -59 ‰ (July) (Fig. 10, Fig. S4). The effect of vapor transport is visible only in 'old' layers (up to the surface in January; from 11 cm depth downward in December), which were originally homogeneous in terms of δ^{18}O.

4.2.4 Ten-years simulation at Dome C

We run a simulation over 10 years at Dome C, with variable δ^{18}O in the precipitation. Over these 10 years, about 1 m of snow is deposited**.** At the end of the simulation, the vertical profile of δ^{18}O in the new layers has an average value of -49.8 ‰, and a half-amplitude of 5.52 ‰ (Fig. 11). Thus the initial signal in the snow is already different from the initial signal in the precipitation (average value of -53.2 ‰, half-amplitude of 8.6 ‰), due to precipitation intermittency, and also to the vertical resolution chosen for the model (layer thickness ~2.5 cm). The values recorded for summer layers (above -45 ‰) reflect the average summer temperatures, whereas the values recorded for winter layers (below -50 ‰) are biased toward warm events (leading to an increase of +6 ‰ of δ^{18}O compared to the value expected with constant precipitation throughout the year).

As expected, the maxima and minima of δ^{18}O are further reduced as a result of diffusion driven by temperature gradients. The effect of vapor transport is relatively small so that to help its visualization, we selected three summers (2002, 2004, 2006) and one winter (2000), and followed the evolution of δ^{18}O in the layers corresponding to the deposited snow during these seasons (Fig. 11d).

For the layer deposited during winter 2000, there is an increase in δ^{18}O values of about +0.8 ‰ over ten years. The slope is irregular, with the strongest increases occurring during summers (Nov.-Feb.) when vapor transport is maximal. The slope is also stronger when the layer is still close to the surface, probably because of the stronger temperature gradients in the first centimeters of snow (Fig. 11a; Sect. 4.3.1.). For the layers deposited during the summers, the evolution of $\delta^{18}O$ values is symmetric to the one observed for winter 2000.

Over 10 years (2000-2009), the amplitude thus decreases by about 1.6 ‰ (0.8 ‰ for the half-amplitude). This corresponds to a decrease of 14 % relative to the initial amplitude in the snow layers. This is higher than the 8 % attenuation (or 9.5 %, when including diffusion caused by temperature gradients) modelled in Greenland (Sect. 4.1.). However, the comparison between the two sites is not straightforward, because of differences in temperature and accumulation counteracting each other. On the one hand, at GRIP, the diffusion is forced by low vertical gradients of $\delta^{18}O$ of the order of 24 ‰ m^{-1}, much smaller than the typical $\delta^{18}O$ gradients at Dome C (110 ‰ m^{-1}). On the other hand, the temperature at GRIP is higher than at Dome C (241 K instead of 220 K), thus favoring diffusion.

4.3 Sensitivity tests for duration of recrystallization

We have shown above that attenuation of the isotopic signal seems too small at least for the GRIP site. In parallel, some parameters of the model, especially for the parameterization of grain renewal, could only loosely be estimated leading to a large uncertainty in the attenuation modeling. In this section, we perform some sensitivity tests to quantify how $\delta^{18}O$ attenuation can be increased by exploring the uncertainty range on the renewal of the snow grain. Indeed, the assumed values for the ratio between the mass of grain surface and the total mass of the grain (τ), or for the periodicity of mixing between these two compartments ($\Delta t_{surf/center}$) may have been under or over-estimated.

The sensitivity tests are first designed for Greenland sites, run for 6 months, with initial amplitude of the sinusoidal $\delta^{18}O$ signal of 16 ‰, and a fixed temperature of 241 K in all the layers (Fig. 12). First, we use a periodicity of mixing $\Delta t_{surf/center}$ of 15 days (more precisely, this mixing occurs on the second and 16th of each month) and vary the value for the mass ratio between the grain surface compartment and the total mass of the grain (τ): $1 \cdot 10^{-6}$, $5 \cdot 10^{-4}$, $3.3 \cdot 10^{-2}$. Then, we use the usual value of $5\ 10^{-4}$ for τ, and change the periodicity of the mixing to 2 days.

- In the first case ($\tau = 1\ 10^{-6}$, mixing of 15 days, Fig. 12a), the grain surface compartment is very small, and its original sinusoidal $\delta^{18}O$ profile disappears in less than one day due to exchanges with vapor. The impact on grain center is

Geosci. Model Dev. Discuss., https://doi.org/10.5194/gmd-2017-217
Manuscript under review for journal Geosci. Model Dev.
Discussion started: 26 October 2017

then very small (attenuation of ~1.7 10^{-4} ‰ over 6 months). In this case, the attenuation due to diffusion is even reduced compared to the results displayed above.

- In the second case (τ= 5 10^{-4}, mixing of 15 days, Fig. 12b), the grain surface compartment is larger, the attenuation is slower, and half of the original amplitude still remains at the end of the 15 days. The impact on the grain center compartment is clearly visible (attenuation of 4.9 10^{-2} ‰ after 6 months).
- In the third case (τ= 3.3 10^{-2}, mixing of 15 days, Fig. 12c), the attenuation of the sinusoidal signal in the grain surface compartment is only of 1 % because the grain surface compartment is very large. On opposite, attenuation in the grain center is quite large, i.e. 7.2 10^{-2} ‰ after 6 months.
- In the fourth case (τ= 5 10^{-4}, mixing of 2 days, Fig. 12d), the attenuation in grain center is similar to the attenuation observed in the third case (7.5 10^{-2} ‰ in 6 months).

The results of these sensitivity tests suggest that the impact of vapor transfer on the grain center isotopic compositions is maximized when the grain surface compartment is large (τ=3.3 10^{-2}) and/or refreshed often ($\Delta t_{surf/center}$=2 days). They also show clearly that using a small grain surface compartment (τ= 1 10^{-6}) drastically reduces the impact on the grain center isotopic values. However, our best estimates for τ and $\Delta t_{surf/center}$ were not chosen randomly (see Sect. 3.1.3.), and moreover, the use of τ=3.3 10^{-2} or $\Delta t_{surf/center}$=2 days lead to an increase of the δ^{18}O attenuation by only a third (see above), which does not bridge the gap between our model output and the data.

At Dome C (mean temperature of 220 K in the simulation), sensitivity tests show that we can increase the attenuation by a factor of 3 by reducing the mixing time from 15 to 2 days. Similarly, if the ratio τ is put at 3.3 10^{-2} instead of 5 10^{-4}, a maximum attenuation of 4.3 ‰ instead of 0.45 ‰ is attained over 6 years. Thus at Dome C and in opposite to GRIP, the values of τ and $\Delta t_{surf/center}$ can affect strongly the attenuation obtained. This greater sensitivity at Dome C could result from the influence of temperature gradients (in Greenland the impact of temperature gradients on attenuation is minor), as well as from steeper δ^{18}O gradients caused by the low accumulation. Indeed, the layer thickness (2 cm in the first meter) corresponds to ~4 points per year at Dome C, but 35 points per year at GRIP.

4.4 Additional missing processes

In the previous sections, we have seen that within the uncertainty range of badly constrained parameters, it is difficult to reconcile data and model output for GRIP. We thus believe that other processes should probably be considered to explain the remaining attenuation. First, previous studies have suggested that water vapor diffusivity within the snow porosity may be underestimated by a factor of 5 (Colbeck, 1983), but this is debated (Calonne et al., 2014). Second, ventilation is an additional process that has already been implemented in the snow water isotopic model of Town et al. (2008) and Neumann (2003). Because of strong porosity and sensitivity to surface wind and relief, ventilation is probably as important as diffusion in the top of the firn, even if diffusion is expected to be more effective at greater depths. Indeed, for the Dome C simulation (Fig. 11***)*,** the slope $d(\delta^{18}O)/dz$ decreases slowly, indicating that diffusion remains almost as active at 60 centimeters than at 10 centimeters depth. Neumann (2003) indicates that at Taylor Mouth the diffusion becomes the only process of vapor transport below 2 meters depth. For Dome C, we compute an average speed due to diffusion of 3 10^{-6} ms^{-1} (for a temperature gradient of 3 °C m^{-1}), which is comparable to air speed due to wind pumping of about 3 10^{-6} ms^{-1} within the top meters of snow at WAIS (Buizert and Severinghaus, 2016). We conclude that, in as much as these results can be applied to Dome C, the two processes would have comparable impact at this site in the first meters of snow. The next step for Crocus-iso development is thus to implement ventilation.

5. Conclusions and perspectives

Water vapor transport (diffusion) and water isotopes have been implemented in the Crocus snow model enabling depicting the temporal $\delta^{18}O$ variations in the top 10 m of the snow in response to new precipitation, evolution of temperature gradient in the snow and densification. We have implemented water vapor and isotopic diffusion between layers at the centimetric scale taking into account two compartments in the snow grain (surface snow in equilibrium with interstitial water vapor and inner grain only exchanging slowly with the surface compartment). We parameterized the speed of diffusion through the renewal time of a snow grain and proportion of the two snow grain compartments.

Our approach based on a detailed snow model makes it possible to investigate at fine scale the processes explaining the variations of density and $\delta^{18}O$ in the firn with evolution of the temperature gradient, new snow accumulation and compaction event linked to wind drift. Over the first 30 cm, the density variations are mainly driven by compaction events linked to wind drift. Vapor transport and long term compaction have secondary effects. Below 30 cm, wind drift driven compaction is no more visible. Because of strong temperature gradient and low density, water vapor transport will have a significant effect down to 60 cm. δ^{18}O is primary driven by variations in δ^{18}O of precipitation as expected. The seasonal variations are then attenuated by water vapor transport and diffusion against isotopic gradients, with an increase of these effects at higher temperature (i.e. summer periods).

From 10 years simulations of the Crocus-iso model both at Summit Greenland and Dome C Antarctica, we have estimated the post-deposition attenuation of the annual δ^{18}O signal in the snow to about 8-14 % through diffusion. This attenuation is smaller than the one obtained from isotopic data on shallow cores in Greenland suggesting missing processes in the Crocus model when implementing water vapor. It is also significantly smaller than the diffusion implemented by Johnsen et al. (2000) but some studies have suggested that the Johnsen isotopic diffusivity is too strong (Denux, 1996 ; Van der Wel et al., 2015).

We see our study as first step toward a complete post-deposition modelling of water isotope variations. Indeed, several other developments are foreseen in this model. First, wind pumping is currently not implemented in the Crocus model. This effect, implemented in the approach of Neumann (2003) and Town et al. (2008) is expected to have a contribution as large as the effect of diffusion for the post-deposition isotopic variations. Second, in low accumulation sites like Dome C, wind scouring has probably an important effect on the evolution of the δ^{18}O signal in depth through a reworking of the top snow layers (Libois et al., 2014). This effect has not been considered here. It could also play a role in the preservation of anomalously strong δ^{18}O peaks at Dome C (Denux, 1996).

Other short term developments concern the implementation of the exchange of water vapor with the atmosphere through hoar deposition. This is particularly timely since many recent studies have studied the parallel evolution of isotopic composition of water vapor and surface snow during summer both in Greenland and Antarctica (Steen-Larsen et al., 2014; Ritter et al., 2016; Casado et al., 2016a; 2016b).

Another aspect is to look at the post-deposition d-excess and ^{17}O-excess variations in snow pits. Indeed, recent studies have shown that the relationship between ^{17}O-excess and δ^{18}O is not the same when looking at precipitation samples and snow pits samples in East Antarctica questioning the influence of diffusion within the snowpack on second order parameters such as ^{17}O-excess (Touzeau et al, 2016). Indeed, ^{17}O-excess is strongly influenced by kinetic diffusion driven fractionation which may be quantified by the implementation of ^{17}O-excess in our Crocus-iso model.

Code availability

The code used in the manuscript is a development of the SURFEX/Crocus model, hosted at CNRM/GAME. Both the initial code and the one used in the manuscript are open source and hosted on a svn server at CNRM/GAME. Users may obtain access to the svn following first the procedure described at: https://opensource.umr-cnrm.fr/projects/snowtools/wiki/Procedure_for_new_users. The specific version of the code corresponding to the results presented can then be retrieved from the svn branch at: http://svn.cnrm-game-meteo.fr/projets/surfex/branches/touzeau_dev using revision 4805. The climate forcing required to perform the runs is available as a supplement.

Author contribution

S. Morin wrote the new module of vapor diffusion. A. Touzeau inserted isotopes and isotope transport into the numerical code with help of S. Morin for numerical issues and physics, and help from A. Landais for concepts and hypotheses of the theory of isotopes. G. Picard and L. Arnaud provided information and references on snow microstructure and microphysics as well as direct field experience on site meteorology and accumulation conditions. A. Touzeau run the simulations, and interpreted the results. A. Touzeau and A. Landais wrote the manuscript. All the authors corrected the manuscript.

Competing interests

The authors declare that they have no conflict of interest.

Acknowledgements

The research leading to these results has received funding from the European Research Council under the European Union's Seventh Framework Programme (FP7/2007-30 2013)/ERC grant agreement no. 306045. We want to acknowledge A. Orsi and M. Casado from LSCE, who contributed to this work through fertile discussions of the model contents and its applications. We are grateful to M. Casado and C. Bréant for providing snow pit temperature and density profiles as well as firn density profiles for model initialization. We would like to thank D. Roche for his advice during model development, as well as on how to make the code available. We are also indebted to J.-Y. Peterschmidt, who provided continual help and useful tutorials on Fortran and Python languages. We thank M. Lafaysse and V. Vionnet at CNRM/CEN for help with the model and meteorological driving data. CNRM/CEN and IGE are part of LabEX OSUG@2020.

References

Albert, M. R. and Hardy, J. P.: Ventilation experiments in seasonal snow cover, IAHS Publications-Series of Proceedings and Reports-Intern Assoc Hydrological Sciences, 228, 41-50, 1995.

Albert, M. R. and McGilvary, W. R.: Thermal effects due to air flow and vapor transport in dry snow, Journal of Glaciology, 38, 273-281, 1992.

Albert, M. R. and Shultz, E. F.: Snow and firn properties and air–snow transport processes at Summit, Greenland, Atmospheric Environment, 36, 2789-2797, 2002.

Albert, M. R., Grannas, A. M., Bottenheim, J., Shepson, P. B., and Perron, F. E.: Processes and properties of snow–air transfer in the high Arctic with application to interstitial ozone at Alert, Canada, Atmospheric Environment, 36, 2779-2787, 2002.

Altnau, S., Schlosser, E., Isaksson, E., and Divine, D.: Climatic signals from 76 shallow firn cores in Dronning Maud land, East Antarctica, The Cryosphere, 9, 925-944, 2015.

Barkan, E. and Luz, B.: Diffusivity fractionations of $H_2{}^{16}O/H_2{}^{17}O$ and $H_2{}^{16}O/H_2{}^{18}O$ in air and their implications for isotope hydrology, Rapid Communications in Mass Spectrometry, 21, 2999-3005, 2007.

Bolzan, J. F. and Pohjola, V. A.: Reconstruction of the undiffused seasonal oxygen isotope signal in central Greenland ice cores, Journal of Geophysical Research: Oceans, 105, 22095-22106, 2000.

Bréant, C., Martinerie, P., Orsi, A., Arnaud, L., and Landais, A.: Modelling the firn thickness evolution during the last deglaciation: constrains on sensitivity to temperature and impurities, Clim. Past Discuss., 2016, 1-36, 2016.

Brun, E. and Touvier, F.: Etude expérimentale de la convection thermique dans la neige, Le Journal de Physique Colloques, 48, C1-257-C1-262, 1987.Brun, E., David, P., Sudul, M., and Brunot, G.: A numerical model to simulate snow-cover stratigraphy for operational avalanche forecasting, Journal of Glaciology, 38, 13-22, 1992.

Brun, E., Six, D., Picard, G., Vionnet, V., Arnaud, L., Bazile, E., Boone, A., Bouchard, A., Genthon, C., and Guidard, V.: Snow/atmosphere coupled simulation at Dome C, Antarctica, Journal of Glaciology, 57, 721-736, 2011.

Buizert, C. and Severinghaus, J. P.: Dispersion in deep polar firn driven by synoptic-scale surface pressure variability, The Cryosphere, 10, 2099-2111, 2016.

Calonne, N., Geindreau, C., and Flin, F.: Macroscopic modeling for heat and water vapor transfer in dry snow by homogenization, The Journal of Physical Chemistry B, 118, 13393-13403, 2014.

Calonne, N., Geindreau, C., and Flin, F.: Macroscopic modeling of heat and water vapor transfer with phase change in dry snow based on an upscaling method: Influence of air convection, Journal of Geophysical Research: Earth Surface, 120, 2476-2497, 2015.

Carmagnola, C. M., Morin, S., Lafaysse, M., Domine, F., Lesaffre, B., Lejeune, Y., Picard, G., and Arnaud, L.: Implementation and evaluation of prognostic representations of the optical diameter of snow in the SURFEX/ISBA-Crocus detailed snowpack model, The Cryosphere, 8, 417-437, 2014.

Casado, M., Landais, A., Masson-Delmotte, V., Genthon, C., Kerstel, E., Kassi, S., Arnaud, L., Picard, G., Prié, F., Cattani, O., Steen-Larsen, H. C., Vignon, E., and Cermak, P.: Continuous measurements of isotopic composition of water vapour on the East Antarctic Plateau, Atmos. Chem. Phys. Discuss., 16, 8521-8538, 2016a.

Casado, M., Landais, A., Picard, G., Münch, T., Laepple, T., Stenni, B., Dreossi, G., Ekaykin, A., Arnaud, L., Genthon, C., Touzeau, A., Masson-Delmotte, V., and Jouzel., J.: Archival of the water stable isotope signal in East Antarctic ice cores, The Cryosphere Discussions, doi:10.5194/tc-2016-263, 2016b.

Colbeck, S. C.: Theory of metamorphism of dry snow, Journal of Geophysical Research, 88, 5475-5482, 1983.

Colbeck, S. C.: Air movement in snow due to wind pumping, Journal of Glaciology, 35, 209-213, 1989.

Dahl-Jensen, D., Johnsen, S., Hammer, C., Clausen, H., and Jouzel, J.: Past accumulation rates derived from observed annual layers in the GRIP ice core from Summit, Central Greenland. In: Ice in the climate system, Springer, 1993.

Dee, D. P., Uppala, S. M., Simmons, A. J., Berrisford, P., Poli, P., Kobayashi, S., Andrae, U., Balmaseda, M. A., Balsamo, G., Bauer, P., Bechtold, P., Beljaars, A. C. M., van de Berg, L., Bidlot, J., Bormann, N., Delsol, C., Dragani, R., Fuentes, M., Geer, A. J., Haimberger, L., Healy, S. B., Hersbach, H., Hólm, E. V., Isaksen, L., Kållberg, P., Köhler, M., Matricardi, M., McNally, A. P., Monge-Sanz, B. M., Morcrette, J. J., Park, B. K., Peubey, C., de Rosnay, P., Tavolato, C., Thépaut, J. N., and Vitart, F.: The ERA-Interim reanalysis: configuration and performance of the data assimilation system, Quarterly Journal of the Royal Meteorological Society, 137, 553-597, 2011.

Delmotte, M., Masson, V., Jouzel, J., and Morgan, V. I.: A seasonal deuterium excess signal at Law Dome, coastal eastern Antarctica: A Southern Ocean signature, Journal of Geophysical Research: Atmospheres, 105, 7187-7197, 2000.

Denux, F.: Diffusion du signal isotopique dans le névé et dans la glace. Implication pour l'échantillonnage., PhD, Geosciences, Université Joseph Fourier-Grenoble 1, Grenoble, 243 pp., 1996.

Domine, F., Taillandier, A. S., Cabanes, A., Douglas, T. A., and Sturm, M.: Three examples where the specific surface area of snow increased over time, The Cryosphere, 3, 31-39, 2009.

Domine, F., Morin, S., Brun, E., Lafaysse, M., and Carmagnola, C. M.: Seasonal evolution of snow permeability under equi-temperature and temperature-gradient conditions, The Cryosphere, 7, 1915-1929, 2013.

Ekaykin, A. A., Lipenkov, V. Y., Barkov, N. I., Petit, J. R., and Masson-Delmotte, V.: Spatial and temporal variability in isotope composition of recent snow in the vicinity of Vostok station, Antarctica: implications for ice-core record interpretation, Annals of Glaciology, 35, 181-186, 2002.

Ekaykin, A., Hondoh, T., Lipenkov, V. Y., and Miyamoto, A.: Post-depositional changes in snow isotope content: preliminary results of laboratory experiments, Climate of the Past Discussions, 5, 2239-2267, 2009.

Ekaykin, A. A., Kozachek, A. V., Lipenkov, V. Y., and Shibaev, Y. A.: Multiple climate shifts in the Southern hemisphere over the past three centuries based on central Antarctic snow pits and core studies, Annals of Glaciology, 55, 259-266, 2014.

Ellehoj, M. D., Steen-Larsen, H. C., Johnsen, S. J., and Madsen, M. B.: Ice-vapor equilibrium fractionation factor of hydrogen and oxygen isotopes: Experimental investigations and implications for stable water isotope studies, Rapid Communications in Mass Spectrometry, 27, 2149-2158, 2013.

EPICA comm. members: Eight glacial cycles from an Antarctic ice core, Nature, 429, 623-628, 2004.

EPICA comm. members: One-to-one coupling of glacial climate variability in Greenland and Antarctica, Nature, 444, 195-198, 2006.

Fisher, D. A. and Koerner, R. M.: Signal and noise in four ice-core records from the Agassiz Ice Cap, Ellesmere Island, Canada: details of the last millennium for stable isotopes, melt and solid conductivity, The Holocene, 4, 113-120, 1994.

Epstein, S. and Sharp, R. P.: Six-year record of oxygen and hydrogen isotope variations in South Pole firn, Journal of Geophysical Research, 70, 1809-1814, 1965.

Flanner, M. G. and Zender, C. S.: Linking snowpack microphysics and albedo evolution, Journal of Geophysical Research: Atmospheres, 111, D12208, doi:10.1029/2005JD006834, 2006.

Fréville, H., Brun, E., Picard, G., Tatarinova, N., Arnaud, L., Lanconelli, C., Reijmer, C., and van den Broeke, M.: Using MODIS land surface temperatures and the Crocus snow model to understand the warm bias of ERA-Interim reanalyses at the surface in Antarctica, The Cryosphere, 8, 1361-1373, 2014.

Frezzotti, M., Pourchet, M., Flora, O., Gandolfi, S., Gay, M., Urbini, S., Vincent, C., Becagli, S., Gragnani, R., and Proposito, M.: Spatial and temporal variability of snow accumulation in East Antarctica from traverse data, Journal of Glaciology, 51, 113-124, 2005.

Friedman, I., Benson, C., and Gleason, J.: Isotopic changes during snow metamorphism, Stable isotope geochemistry: a tribute to Samuel Epstein, 1991. 211-221, 1991.

Gallet, J.-C., Domine, F., Arnaud, L., Picard, G., and Savarino, J.: Vertical profile of the specific surface area and density of the snow at Dome C and on a transect to Dumont D'Urville, Antarctica-albedo calculations and comparison to remote sensing products, The Cryosphere, 5, 631-649, 2011.

Gay, M., Fily, M., Genthon, C., Frezzotti, M., Oerter, H., and Winther, J.-G.: Snow grain-size measurements in Antarctica, Journal of Glaciology, 48, 527-535, 2002.

Genthon, C., Six, D., Gallée, H., Grigioni, P., and Pellegrini, A.: Two years of atmospheric boundary layer observations on a 45-m tower at Dome C on the Antarctic plateau, Journal of Geophysical Research: Atmospheres, 118, 3218-3232, 2013.

Genthon, C., Six, D., Scarchilli, C., Ciardini, V., and Frezzotti, M.: Meteorological and snow accumulation gradients across Dome C, East Antarctic plateau, International Journal of Climatology, 36, 455-466, 2016.

Gkinis, V., Simonsen, S. B., Buchardt, S. L., White, J. W. C., and Vinther, B. M.: Water isotope diffusion rates from the NorthGRIP ice core for the last 16,000 years – Glaciological and paleoclimatic implications, Earth and Planetary Science Letters, 405, 132-141, 2014.

Guillevic, M., Bazin, L., Landais, A., Kindler, P., Orsi, A., Masson-Delmotte, V., Blunier, T., Buchardt, S., Capron, E., and Leuenberger, M.: Spatial gradients of temperature, accumulation and δ^{18}O-ice in Greenland over a series of Dansgaard–Oeschger events, Climate of the Past, 9, 1029-1051, 2013.

Hoshina, Y., Fujita, K., Nakazawa, F., Iizuka, Y., Miyake, T., Hirabayashi, M., Kuramoto, T., Fujita, S., and Motoyama, H.: Effect of accumulation rate on water stable isotopes of near-surface snow in inland Antarctica, Journal of Geophysical Research, 119, 274-283, 2014.

Johnsen, S.: Stable isotope homogenization of polar firn and ice, Isotopes and impurities in snow and ice, 1, 210-219, 1977.

Johnsen, S. J., Dahl-Jensen, D., Dansgaard, W., and Gundestrup, N.: Greenland palaeotemperatures derived from GRIP bore hole temperature and ice core profiles, Tellus, 47B, 624-629, 1995.

Johnsen, S. J., Clausen, H. B., Cuffey, K. M., Hoffmann, G., Schwander, J., and Creyts, T.: Diffusion of stable isotopes in polar firn and ice: the isotope effect in firn diffusion, Physics of ice core records, 159, 121-140, 2000.

Joos, F. and Spahni, R.: Rates of change in natural and anthropogenic radiative forcing over the past 20,000 years, Proceedings of the National Academy of Sciences, 105, 1425-1430, 2008.

Jouzel, J., Masson-Delmotte, V., Stiévenard, M., Landais, A., Vimeux, F., Johnsen, S. J., Sveinbjörnsdottir, A. E., and White, J. W. C.: Rapid deuterium-excess changes in Greenland ice cores: a link between the ocean and the atmosphere, Comptes Rendus Geoscience, 337, 957-969, 2005.

Jouzel, J., Masson-Delmotte, V., Cattani, O., Dreyfus, G., Falourd, S., Hoffmann, G., Minster, B., Nouet, J., Barnola, J. M., Chappellaz, J., Fischer, H., Gallet, J. C., Johnsen, S., Leuenberger, M., Loulergue, L., Luethi, D., Oerter, H., Parrenin, F., Raisbeck, G., Raynaud, D., Schilt, A., Schwander, J., Selmo, E., Souchez, R., Spahni, R., Stauffer, B., Steffensen, J. P., Stenni, B., Stocker, T. F., Tison, J. L., Werner, M., and Wolff, E. W.: Orbital and millennial Antarctic climate variability over the past 800,000 years, Science, 317, 793-796, 2007.

Kaempfer, T. U., Schneebeli, M., and Sokratov, S. A.: A microstructural approach to model heat transfer in snow, Geophysical Research Letters, 32, L21503, doi:10.1029/2005GL023873, 2005.

Kawamura, K., Parrenin, F., Lisiecki, L., Uemura, R., Vimeux, F., Severinghaus, J. P., Hutterli, M. A., Nakazawa, T., Aoki, S., Jouzel, J., Raymo, M. E., Matsumoto, K., Nakata, H., Motoyama, H., Fujita, S., Goto-Azuma, K., Fujii, Y., and Watanabe, O.: Northern Hemisphere forcing of climatic cycles in Antarctica over the past 360,000 years, Nature, 448, 912-916, 2007.

Laepple, T., Werner, M., and Lohmann, G.: Synchronicity of Antarctic temperatures and local solar insolation on orbital timescales, Nature, 471, 91, 2011.

Landais, A., Barkan, E., and Luz, B.: Record of δ^{18}O and ^{17}O-excess in ice from Vostok Antarctica during the last 150,000 years, Geophysical Research Letters, 35, L02709, 2008.

Lefebre, F., Gallée, H., van Ypersele, J.-P., and Greuell, W.: Modeling of snow and ice melt at ETH Camp (West Greenland): A study of surface albedo, Journal of Geophysical Research: Atmospheres, 108, D8-4231, doi:10.1029/2001JD001160, 2003.

Libois, Q., Picard, G., Arnaud, L., Morin, S., and Brun, E.: Modeling the impact of snow drift on the decameter-scale variability of snow properties on the Antarctic Plateau, Journal of Geophysical Research: Atmospheres, 119, 11662-11681, 2014.

Libois, Q., Picard, G., Arnaud, L., Dumont, M., Lafaysse, M., Morin, S., and Lefebvre, E.: Summertime evolution of snow specific surface area close to the surface on the Antarctic Plateau, The Cryosphere, 9, 2383-2398, 2015.

Lorius, C., Jouzel, J., Ritz, C., Merlivat, L., Barkov, N. I., Korotkevich, Y. S., and Kotlyakov, V. M.: A 150,000-year climatic record from Antarctic ice, Nature, 316, 591-596, 1985.

Lu, G. and DePaolo, D. J.: Lattice Boltzmann simulation of water isotope fractionation during ice crystal growth in clouds, Geochimica et Cosmochimica Acta, 180, 271-283, 2016.

Magand, O., Frezzotti, M., Pourchet, M., Stenni, B., Genoni, L., and Fily, M.: Climate variability along latitudinal and longitudinal transects in East Antarctica, Annals of Glaciology, 39, 351-358, 2004.

Mann, M. E. and Jones, P. D.: Global surface temperatures over the past two millennia, Geophysical Research Letters, 30, 1820, doi:10.1029/2003GL017814, 2003.Masson-Delmotte, V., Delmotte, M., Morgan, V., Etheridge, D., van Ommen, T., Tartarin, S., and Hoffmann, G.: Recent southern Indian Ocean climate variability inferred from a Law Dome ice core: new insights for the interpretation of coastal Antarctic isotopic records, Clim Dyn, 21, 153-166, 2003.

Masson-Delmotte, V., Landais, A., Stievenard, M., Cattani, O., Falourd, S., Jouzel, J., Johnsen, S. J., Dahl-Jensen, D., Sveinsbjornsdottir, A., White, J. W. C., Popp, T., and Fischer, H.: Holocene climatic changes in Greenland: Different deuterium excess signals at Greenland Ice Core Project (GRIP) and NorthGRIP, Journal of Geophysical Research: Atmospheres, 110, 1-13, 2005.

Masson-Delmotte, V., Buiron, D., Ekaykin, A., Frezzotti, M., Gallée, H., Jouzel, J., Krinner, G., Landais, A., motoyama, H., Oerter, H., Pol, K., Pollard, D., Ritz, C., Schlosser, Z., Sime, L. C., Sodemann, H., Stenni, B., Uemura, R., and Vimeux, F.: A comparison of the present and last interglacial periods in six Antarctic ice cores, Clim. Past, 7, 397-423, 2011.

Masson-Delmotte, V., Steen-Larsen, H., Ortega, P., Swingedouw, D., Popp, T., Vinther, B., Oerter, H., Sveinbjörnsdottir, A., Gudlaugsdottir, H., and Box, J.: Recent changes in north-west Greenland climate documented by NEEM shallow ice core data and simulations, and implications for past-temperature reconstructions, The Cryosphere Discussions, 2015. 1481-1504, 2015.Mayewski, P. and Goodwin, I.: Antarctic's role pursued in global climate change, Eos, Transactions American Geophysical Union, 80, 398-400, 1999.

Morse, D. L., Waddington, E. D., Marshall, H.-P., Neumann, T. A., Steig, E. J., Dibb, J. E., Winebrenner, D. P., and Arthern, R. J.: Accumulation Rate Measurements at Taylor Dome, East Antarctica: Techniques and Strategies for Mass Balance Measurements in Polar Environments, Geografiska Annaler: Series A, Physical Geography, 81, 683-694, 1999.

Neumann, T. A.: Effects of firn ventilation on geochemistry of polar snow, PhD, Department of Earth and Space Sciences, University of Washington, Washington, 223 pp., 2003.

Neumann, T. A. and Waddington, E. D.: Effects of firn ventilation on isotopic exchange, Journal of Glaciology, 50, 183-194, 2004.

Neumann, T. A., Waddington, E. D., Steig, E. J., and Grootes, P. M.: Non-climate influences on stable isotopes at Taylor Mouth, Antarctica, Journal of Glaciology, 51, 248-258, 2005.

Neumann, T., Albert, M., Lomonaco, R., Engel, C., Courville, Z., and Perron, F.: Experimental determination of snow sublimation rate and stable-isotopic exchange, Annals of Glaciology, 49, 1-6, 2008.

Neumann, T. A., Albert, M. R., Engel, C., Courville, Z., and Perron, F.: Sublimation rate and the mass-transfer coefficient for snow sublimation, International Journal of Heat and Mass Transfer, 52, 309-315, 2009.Petit, J. R., Jouzel, J., Pourchet, M., and Merlivat, L.: A detailed study of snow accumulation and stable isotope content in Dome C (Antarctica), Journal of Geophysical Research, 87, 4301-4308, 1982.

Petit, J. R., Jouzel, J., Raynaud, D., Barkov, N. I., Barnola, J. M., Basile, I., Bender, M., Chappellaz, J., Davis, M., Delaygue, G., Delmotte, M., Kotlyakov, V. M., Legrand, M., Lipenkov, V. Y., Lorius, C., Pepin, L., Ritz, C., Saltzman, E., and Stievenard, M.: Climate and atmospheric history of the past 420,000 years from the Vostok ice core, Antarctica, Nature, 399, 429-436, 1999.

Picard, G., Arnaud, L., Panel, J. M., and Morin, S.: Design of a scanning laser meter for monitoring the spatio-temporal evolution of snow depth and its application in the Alps and in Antarctica, The Cryosphere, 10, 1495-1511, 2016.

Pinzer, B. R., Schneebeli, M., and Kaempfer, T. U.: Vapor flux and recrystallization during dry snow metamorphism under a steady temperature gradient as observed by time-lapse micro-tomography, The Cryosphere, 6, 1141-1155, 2012.

Ramseier, R. O.: Self-diffusion of tritium in natural and syntehtic ice monocrystals, Journal of Applied Physics, 38, 2553-2556, 1967.

Ritter, F., Steen-Larsen, H. C., Werner, M., Masson-Delmotte, V., Orsi, A., Behrens, M., Birnbaum, G., Freitag, J., Risi, C., and Kipfstuhl, S.: Isotopic exchange on the diurnal scale between near-surface snow and lower atmospheric water vapor at Kohnen station, East Antarctica, The Cryosphere Discuss., 2016, 1-35, 2016.

Schilt, A., Baumgartner, M., Blunier, T., Schwander, J., Spahni, R., Fischer, H., and Stocker, T. F.: Glacial-interglacial and millenial-scale variations in the atmospheric nitrous oxide concentration during the last 8000,000 years, Quaternary Science Reviews, 29, 182-192, 2010.

Schneider, D. P., Steig, E. J., Ommen, T. D. v., Dixon, D. A., Mayewski, P. A., Jones, J. M., and Bitz, C. M.: Antarctic temperatures over the past two centuries from ice cores, Geophysical Research Letters, 33, L16707, 2006.

Shaheen, R., Abauanza, M., Jackson, T. L., McCabe, J., Savarino, J., and Thiemens, M. H.: Tales of volcanoes and El-Niño southern oscillations with the oxygen isotope anomaly of sulfate aerosol, Proceedings of the National Academy of Sciences, 110, 17662-17667, 2013.

Shuman, C. A., Alley, R. B., Anandakrishnan, S., White, J. W. C., Grootes, P. M., and Stearns, C. R.: Temperature and accumulation at the Greenland Summit: Comparison of high-resolution isotope profiles and satellite passive microwave brightness temperature trends, Journal of Geophysical Research: Atmospheres, 100, 9165-9177, 1995.

Shuman, C. A., Steffen, K., Box, J. E., and Stearns, C. R.: A dozen years of temperature observations at the Summit: Central Greenland automatic weather stations 1987–99, Journal of Applied Meteorology, 40, 741-752, 2001.

Sime, L. C., Tindall, J. C., Wolff, E. W., Connolley, W. M., and Valdes, P. J.: Antarctic isotopic thermometer during a CO2 forced warming event, Journal of Geophysical Research, 113, D24119, 2008.

Sjolte, J., Hoffmann, G., Johnsen, S. J., Vinther, B. M., Masson-Delmotte, V., and Sturm, C.: Modeling the water isotopes in Greenland precipitation 1959–2001 with the meso-scale model REMO-iso, Journal of Geophysical Research: Atmospheres, 116, D18105, doi:10.1029/2010JD015287, 2011.

Sokratov, S. A. and Golubev, V. N.: Snow isotopic content change by sublimation, Journal of Glaciology, 55, 823-828, 2009.

Steen-Larsen, H. C., Masson-Delmotte, V., Sjolte, J., Johnsen, S. J., Vinther, B. M., Bréon, F. M., Clausen, H., Dahl-Jensen, D., Falourd, S., and Fettweis, X.: Understanding the climatic signal in the water stable isotope records from the NEEM shallow firn/ice cores in northwest Greenland, Journal of Geophysical Research: Atmospheres, 116, D06108, doi:10.1029/2010JD014311, 2011.

Steen-Larsen, H., Masson-Delmotte, V., Hirabayashi, M., Winkler, R., Satow, K., Prié, F., Bayou, N., Brun, E., Cuffey, K., and Dahl-Jensen, D.: What controls the isotopic composition of Greenland surface snow?, Climate of the Past, 10, 377-392, 2014.

Steig, E. J.: The south-north connection, Nature, 44, 152-153, 2006.

Stenni, B., Jouzel, J., Masson-Delmotte, V., Röthlisberger, R., Castellano, E., Cattani, O., Falourd, S., Johnsen, S. J., Longinelli, A., Sachs, J. P., Selmo, E., Souchez, R., Steffensen, J. P., and Udisti, R.: A late-glacial high-resolution site and source temperature record derived from the EPICA Dome C isotope records (East Antarctica), Earth and Planetary Science Letters, 217, 183-195, 2004.

Stenni, B., Buiron, D., Frezzotti, M., Albani, S., Barbante, C., Bard, E., Barnola, J. M., Baroni, M., Baumgartner, M., Bonazza, M., Capron, E., Castellano, E., Chappellaz, J., Delmonte, B., Falourd, S., Genoni, L., Iacumin, P., Jouzel, J., Kipfstuhl, S., Landais, A., Lemieux-Dudon, B., Maggi, V., Masson-Delmotte, V., Mazzola, C., Minster, B., Montagnat, M., Mulvaney, R., Narcisi, B., Oerter, H., Parrenin, F., Petit, J. R., Ritz, C., Scarchilli, C., Schilt, A., Schupbach, S., Schwander, J., Selmo, E., Severi, M., Stocker, T. F., and Udisti, R.: Expression of the bipolar see-saw in Antarctic climate records during the last deglaciation, Nature Geosci, 4, 46-49, 2011.

Stenni, B., Scarchilli, C., Masson-Delmotte, V., Schlosser, E., Ciardini, V., Dreossi, G., Grigioni, P., Bonazza, M., Cagnati, A., Karlicek, D., Risi, C., Udisti, R., and Valt, M.: Three-year monitoring of stable isotopes of precipitation at Concordia Station, East Antarctica, The Cryosphere, 10, 2415-2428, 2016.

Stichler, W., Schotterer, U., Fröhlich, K., Ginot, P., Kull, C., Gäggeler, H., and Pouyaud, B.: Influence of sublimation on stable isotope records recovered from high-altitude glaciers in the tropical Andes, Journal of Geophysical Research, 106, 22613-22620, 2001.

Taillandier, A.-S., Domine, F., Simpson, W. R., Sturm, M., Douglas, T. A., and Severin, K.: Evolution of the snow area index of the subarctic snowpack in central Alaska over a whole season. Consequences for the air to snow transfer of pollutants, Environmental Science and Technology, 40, 7521-7527, 2006.

Taillandier, A.-S., Domine, F., Simpson, W. R., Sturm, M., and Douglas, T. A.: Rate of decrease of the specific surface area of dry snow: Isothermal and temperature gradient conditions, Journal of Geophysical Research: Earth Surface, 112, doi:10.1029/2006JF000514, 2007.

Touzeau, A., Landais, A., Stenni, B., Uemura, R., Fukui, K., Fujita, S., Guilbaud, S., Ekaykin, A., Casado, M., and Barkan, E.: Acquisition of isotopic composition for surface snow in East Antarctica and the links to climatic parameters, The Cryosphere, 10, 837-852, 2016.

Town, M. S., Warren, S. G., Walden, V. P., and Waddington, E. D.: Effect of atmospheric water vapor on modification of stable isotopes in near-surface snow on ice-sheets, Journal of Geophysical Research, 113, D24303, 2008.

Urbini, S., Frezzotti, M., Gandolfi, S., Vincent, C., Scarchilli, C., Vittuari, L., and Fily, M.: Historical behaviour of Dome C and Talos Dome (East Antarctica) as investigated by snow accumulation and ice velocity measurements, Global and Planetary Change, 60, 576-588, 2008.

van de Berg, W. J., van den Broeke, M. R., Reijmer, C. H., and van Meijgaard, E.: Reassessment of the Antarctic surface mass balance using calibrated output of a regional atmospheric climate model, Journal of Geophysical Research: Atmospheres, 111, D11104, doi:10.1029/2005JD006495, 2006.

van der Wel, L., Been, H., Smeets, P., and Meijer, H.: Constraints on the δ 2 H diffusion rate in firn from field measurements at Summit, Greenland, The Cryosphere, 9, 1089-1103, 2015.

Vimeux, F., Cuffey, K. M., and Jouzel, J.: New insights into Southern Hemisphere temperature changes from Vostok ice cores using deuterium excess correction, Earth and Planetary Science Letters, 203, 829-843, 2002.

Vionnet, V., Brun, E., Morin, S., Boone, A., Faroux, S., Le Moigne, P., Martin, E., and Willemet, J.: The detailed snowpack scheme Crocus and its implementation in SURFEX v7. 2, Geoscientific Model Development, 5, 773-791, 2012.

Waddington, E. D., Steig, E. J., and Neumann, T. A.: Using characteristic times to assess whether stable isotopes in polar snow can be reversibly deposited, Annals of Glaciology, 35, 118-124, 2002.

White, J.W.C., Barlow, L.K., Fisher, D., Grootes, P., Jouzel, J., Johnsen, S.J., Stuiver, M., and Clausen, H.: The climate signal in the stable isotope of Summit, Greenland snow : Results of comparisons with modern climate observations. Journal of Geophysical Research, 102, C12, 26425 - 26439, 1997.

Table 1. Definition of the symbols used.

Symbol	**Description**
Constants	
T_0	Temperature of the triple point of water (K)
R_v	Vapor constant for water (J·kg^{-1}K^{-1})
L_{sub}	Latent heat of sublimation of water (J·m^{-3})
ρ_{v0}	Vapor density at 273.16 K (kg·m^{-3} of air)
D_{ice}	Diffusivity of water molecules in solid ice (m^{2}·s^{-1})
D_v	Diffusivity of vapor in air at 263 K (m^{2}·s^{-1}) (temperature dependency neglected)
ρ_{ice}	Density of ice (kg·m^{-3})
a	Accumulation (m i.e. per year)
R_{moy}	Average snow grain radius (m)
Δt_{sol}	Characteristic time for solid diffusion (s)
$\Delta t_{surf/center}$	Periodicity of the mixing between grain center and grain surface, as a result of grain center translation (s)
1D-variables	
t	Time (s)
n	Layer number from top of the snowpack
$\delta^{18}O_{sf}(t)$	Isotopic composition of oxygen in the snowfall (‰)
T_{air} (t)	Temperature of the air at 2 m (K)
2D-variables	
$h(t,n)$	Height of the center of the snow layer relative to the bottom of the snowpack (m)
$z\ (t,n)$	Depth of the center of the snow layer (m from surface)
$dz\ (t,n)$	Thickness of the snow layer (m)
$T\ (t,n)$	Temperature of the snow layer (K)
$\rho_{sn}\ (t,n)$	Density of the snow layer (kg·m^{-3})
$m_{sn}\ (t,n)$	Mass of the snow layer (kg)
$\rho_v\ (t,n)$	Vapor density at saturation in the porosity of the snow layer (kg·m^{-3} of air)
$D_{eff}\ (t,n)$	Effective diffusivity of vapor in the layer (m^{2}·s^{-1})
δ^{18}O (t,n)	Isotopic composition of oxygen in the snow layer (‰)
$F^{18}(n+1 \rightarrow n)$	Flux of the heavy water molecules (^{18}O) from layer n+1 to layer n (kg· m-^{2}·s^{-1})
$F(n+1 \rightarrow n)$	Vapor flux from layer n+1 to layer n (kg· m-^{2}·s^{-1})
$D_{eff}(t, n \rightarrow n+1)$	Effective interfacial diffusivity between layers n and n+1 (m^{2}·s^{-1})
$R^{*}_{vap\ ini}$	Isotopic ratio in the initial vapor (* is either ^{18}O, ^{17}O or D)
$R^{*}_{surf\ ini}$	Isotopic ratio in the grain surface sub-compartment before vapor individualization
$c^{x}_{vap\ ini}$	Concentration in heavy or light isotope in the initial vapor (^{x} is ^{18}O, ^{17}O , ^{16}O, ^{1}H or D)
α^{*}_{sub}	Fractionation coefficients at equilibrium during sublimation (* is either ^{18}O, ^{17}O or D)
	Fractionation coefficients during condensation (* is either ^{18}O, ^{17}O or D)
α^{*}_{cond}	No fractionation
$\alpha^{*}_{cond\ eff}$	Effective (total) fractionation
$\alpha^{*}_{cond\ kin}$	Kinetic fractionation only
$\alpha^{*}_{cond\ eq}$	Equilibrium fractionation only

$m_{vap\ ini}$	Initial mass of vapor in the porosity (kg)
$m_{surf\ ini}$	Mass of water in the grain surface sub-compartment before vapor individualization (kg)
$m_{surf\ new}$	Mass of water in the grain surface sub-compartment after vapor individualization (kg)
τ	Ratio of between the mass of the grain surface compartment and the mass of total grain
m_{surf}	Mass of grain surface compartment
m_{center}	Mass of grain center compartment
m_{vap}	Mass of vapor in the porosity
V_{tot}	Total volume of the considered layer
Φ	Porosity of the layer
$m_{surf\ ini}^{18}$	Mass of heavy water molecules (^{18}O) in the grain surface before vapor individualization (kg)
$m_{surf\ new}^{18}$	Mass of heavy water molecules (^{18}O) in the grain surface after vapor individualization (kg)
D^{18}/D	Kinetic fractionation of heavy isotope relative to light
$\Delta m_{vap,exc}$	Mass of vapor in excess in the porosity after vapor transport (kg)
$\rho_{sn\ ini}$	Density of the snow layer before vapor transport
$\rho_{sn\ new}$	Density of the snow layer after vapor transport
T_{ini}, T_{new}	Temperature of the snow layer before and after vapor transport

GRIP		
Accumulation	23 cm i.e./yr	Dahl-Jensen et al., 1993
Annual temperature	241 K	Masson-Delmotte et al., 2005
Winter temperature	232 K	(Feb.) Shuman et al., 2001
Summer temperature	261 K	(Aug.) Shuman et al., 2001
Mean δ^{18}O	-35.2‰	Masson-Delmotte et al., 2005
δ^{18}O min	-43 ‰	(2m snowpit) Shuman et al., 1995
δ^{18}O max	-27 ‰	(2m snowpit) Shuman et al., 1995
δ^{18}O /T_{air} slope	0.46 ‰/°C	(2m snowpit) Shuman et al., 1995
DOME C		
Accumulation	2.7 cm i.e./yr	Frezzotti et al., 2005; Urbini et al., 2008
Annual temperature	221 K	Stenni et al., 2016
Min winter T_{air}	199 K	Stenni et al., 2016
Max summer T_{air}	248 K	Stenni et al., 2016
Mean δ^{18}O	-56.4 ‰	Stenni et al., 2016
δ^{18}O min winter	-71.8 ‰	Stenni et al., 2016
δ^{18}O max summer	-40.2 ‰	Stenni et al., 2016
δ^{18}O/ T_{air} slope	0.49 ‰/°C	Stenni et al., 2016

985 **Table 2.** Climate and isotope variability at GRIP (Greenland) and Dome C (Antarctica).

Variable	Equation		Average	Range	
Thickness (m)	dz		$1.2\cdot10^{-1}$	$5\cdot10^{-4}$	$8\cdot10^{-1}$
Density (kg m^{-3})	ρ_{sn}		340	300	460
Temperature (K)	T		225	205	255
Mass (kg)	m_{sn}	$=dz\ \rho_{sn}$	42	0.15	368
Vapor density (kg·m^{-3})	ρ_v	Eq. (7)	$1.8\cdot10^{-5}$	$1.2\cdot10^{-6}$	$4.4\cdot10^{-4}$
Porosity	Φ	$=1-(\rho_{sn}/\rho_i)$	0.63	0.5	0.67
Vapor mass (kg)	m_{vap}	Eq. (10)	$1.3\cdot10^{-6}$	$3\cdot10^{-10}$	$2.4\cdot10^{-4}$
Minimum ratio	τmin	$= 1/10^6$	$1\cdot10^{-6}$	$1\cdot10^{-6}$	$1\cdot10^{-6}$
Maximum ratio	τmax	$=\frac{\rho_v\,\Phi}{\rho_{sn}}\cdot10^6$	$3.3\cdot10^{-2}$	$1.3\cdot10^{-3}$	1

Table 3. Typical thickness, density, temperature and other parameters of the snow layers in the simulations. The definitions of symbols are given in Table1. The ratio τ is the mass ratio between the grain surface compartment and the grain center compartment. It must be chosen within the interval $[10^{-6};\ 10^{6}\cdot(\rho_v\ \Phi/\rho_{sn})]$ to allow exchanges between grain surface compartment and grain center compartment, on the one hand; and between grain surface compartment and vapor compartment on the other hand (see text for details).

Geosci. Model Dev. Discuss., https://doi.org/10.5194/gmd-2017-217
Manuscript under review for journal Geosci. Model Dev.
Discussion started: 26 October 2017

	GRIP simulation		**Dome C simulations**			
N°	1	2	3	4	5	6
Section	4.1.1	4.1.2	4.2.1	4.2.2	4.2.3	4.2.4
Figures	Figure 2	Figure 3	Figure 5 & 6	Figure 7 & 8	Figure 9 & 10	Figure 11
Duration	10 years	10 years	1 year	1 year	1 year	10 years
Period	Jan 2000-Dec 2010	Jan 2001-Dec 2011	Jan-Dec 2001	Jan-Dec 2001	Jan-Dec 2001	Jan 2000-Dec 2010
Atmospheric forcing						
Air T	-	ERA-Interim (GR)	ERA-Interim	ERA-Interim	ERA-Interim	ERA-Interim
Specific humidity	-	ERA-Interim (GR)	ERA-Interim	ERA-Interim	ERA-Interim	ERA-Interim
Air pressure	-	ERA-Interim (GR)	ERA-Interim	ERA-Interim	ERA-Interim	ERA-Interim
Wind velocity	-	ERA-Interim (GR)	ERA-Interim	ERA-Interim	ERA-Interim	ERA-Interim
Snowfall	NO	NO	NO	NO	YES	YES
$\delta^{18}O_{sf}$	-	-	-	-	Function (T)*	Function (T)*
Model configuration						
Initial snow T	Flat profile (241 K)	One-year run initialization (Jan-Dec 2000)	One-year run initialization (Jan-Dec 2000)	One-year run initialization (Jan-Dec 2000)	One-year run initialization (Jan-Dec 2000)	Exponential profile**
Evolution of snow T	Constant	Computed	Computed	Computed	Computed	Computed
Initial snow d18O	Sinusoidal profile***	Sinusoidal profile***	-40 ‰	-40 ‰	-40 ‰	-40 ‰
Wind drift	NO	NO	NO	YES	YES	NO
Homogeneous compaction	NO	NO	NO	YES	YES	NO

995 Table 4. List of simulations described in the article with the corresponding paragraph number. The external atmospheric forcing used for Dome C is ERA-Interim reanalysis (2000-2013). However, the precipitation amounts from ERA-Interim reanalysis are increased by 1.5 times to account for the dry bias in the reanalysis (as in Libois et al., 2014). For the second simulation at GRIP, Greenland meteorological conditions are derived from the atmospheric forcing of Dome C, but the temperature is modified (T_{GRIP}=T_{DC}+15) as well as the longwave down (LW_{GRIP}=LW_{DC}*0.85+60).

* Using data from one year snowfall sampling at Dome C (Stenni et al., 2016; Touzeau et al., 2016), we obtained the following Eq. (15) linking $\delta^{18}O_{sf}$ in the snowfall to the local temperature T_{air}: $\delta^{18}O_{sf} = 0.45 \times (T_{air} - 273.15) - 31.5$.

**The exponential profile of temperature used in simulation 6 is defined using Eq. (19):

$$T(z) = T(10m) + \Delta T \times \exp(-z/z0) + 0.1 \times z \tag{19}$$

with T(10m)=218 K, ΔT=28 K, and $z0$=1.516 m.

It fits well with temperature measurements of midday in January (Casado et al., 2016b).

***The Greenland snowpack has an initial sinusoidal profile of δ^{18}O defined using Eq. (18):

$$\delta^{18}O = -35.5 - 8 \times \sin\left(\frac{2\pi \times z}{a \times \rho_{ice}/\rho_{sn}}\right) \tag{18}$$

(see Table 1 for symbols).

	GRIP sensitivity tests				**Dome C sensitivity tests**				
N°	1	2	3	4	1	2	3	4	5
Section	4.3	4.3	4.3	4.3	4.3	4.3	4.3	4.3	4.3
Figures	Figure 12	Figure 12	Figure 12	Figure 12	Figure 13	Figure 13	Figure 13	Figure 13	Figure 13
Duration	6 months	6 months	6 months	6 months	6 years	6 years	6 years	6 years	6 years
Period	Jan-Jun 2000	Jan-Jun 2000	Jan-Jun 2000	Jan-Jun 2000	Jan 2000-Dec 2005	Jan 2000-Dec 2005	Jan 2000-Dec 2005	Jan 2001-Dec 2006	Jan 2001-Dec 2006
Atmospheric forcing									
Air T	-	-	-	-	-	-	-	ERAI	ERAI
Specific humidity	-	-	-	-	-	-	-	ERAI	ERAI
Air pressure	-	-	-	-	-	-	-	ERAI	ERAI
Wind velocity	-	-	-	-	-	-	-	ERAI	ERAI
Snowfall	NO	NO	NO	NO	NO	NO	NO	NO	NO
$\delta^{18}O_{sf}$	-	-	-	-	-	-	-	-	-
Model configuration									
Initial snow T	Flat (241 K)	Flat (241 K)	Flat (241 K)	Flat (241 K)	Flat (241 K)	Flat (220 K)	Flat (220 K)	One-year run init. (Jan-Dec 2000)	One-year run init. (Jan-Dec 2000)
Evolution of snow T	Cst	Cst	Cst	Cst	Cst	Cst	Cst	Computed	Computed
Initial snow d18O	Sinusoid ***	Sinusoid ***	Sinusoid ***	Sinusoid ***	Sinusoid ****	Sinusoid ****	Sinusoid ****	Sinusoid ****	Sinusoid ****
Wind drift	NO	NO	NO	NO	NO	NO	NO	NO	NO
Homog. compaction	NO	NO	NO	NO	NO	NO	NO	NO	NO
Mass ratio τ	$1\cdot10^{-6}$	$5\cdot10^{-4}$	$3.3\cdot10^{-2}$	$5\cdot10^{-4}$	$5\cdot10^{-4}$	$5\cdot10^{-4}$	$5\cdot10^{-4}$	$5\cdot10^{-4}$	$3.3\cdot10^{-2}$
Δtsurf/center	15 days	15 days	15 days	2 days	2 days	2 days	15 days	15 days	15 days

Geosci. Model Dev. Discuss., https://doi.org/10.5194/gmd-2017-217
Manuscript under review for journal Geosci. Model Dev.
Discussion started: 26 October 2017

Table 5. List of the sensitivity tests performed at GRIP and at Dome C. The external atmospheric forcing used for Dome C is ERA-Interim reanalysis (see Table 4). Cst: constant.

***The Greenland snowpack has an initial sinusoidal profile of δ^{18}O defined using Eq. (18):

$$\delta^{18}O = -35.5 - 8 \times \sin\left(\frac{2\pi \times z}{a \times \rho_{ice}/\rho_{sn}}\right) \tag{18}$$

1015 ****The Dome C snowpack has an initial sinusoidal profile of δ^{18}O defined using Eq. (20):

$$\delta^{18}O = -48.5 - 6.5 \times \sin\left(\frac{2\pi \times z}{a \times \rho_{ice}/\rho_{sn}}\right) \tag{20}$$

Refer to Table1 for a list of symbols.

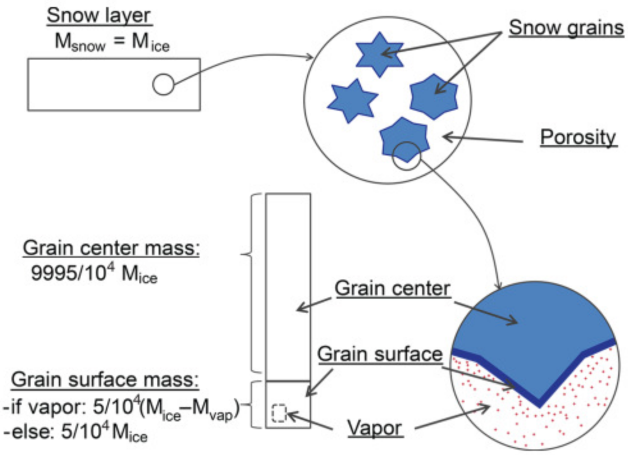

Figure 1. Splitting of the snow layer into two compartments, grain center and grain surface, with a constant mass ratio between them. The vapor compartment is a sub-compartment inside the grain surface compartment, and is only defined at specific steps of the model.

Geosci. Model Dev. Discuss., https://doi.org/10.5194/gmd-2017-217
Manuscript under review for journal Geosci. Model Dev.
Discussion started: 26 October 2017

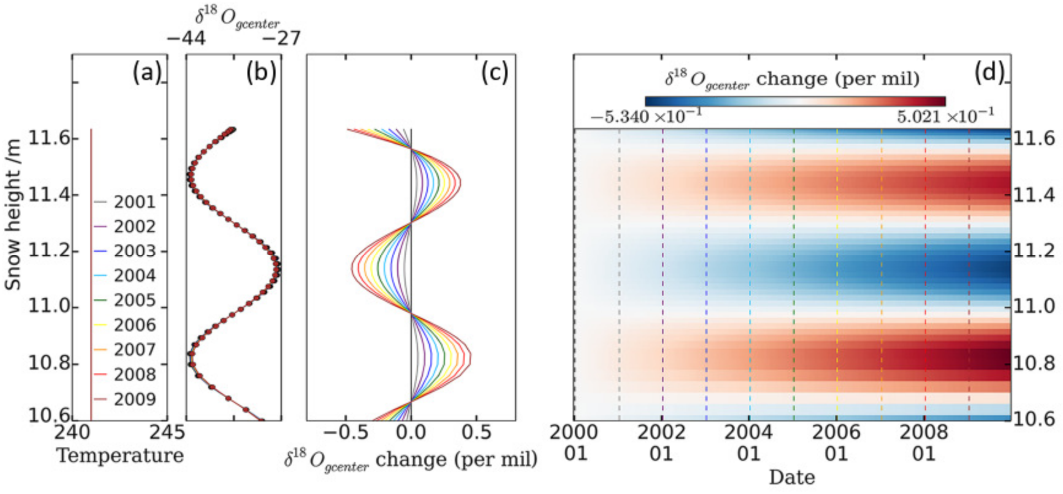

Figure 2. Simulation of the attenuation of the seasonal $\delta^{18}O_{gcenter}$ variation caused by diffusion against isotopic gradients in vapor phase over 10 years (homogeneous and constant temperature of 241 K, original signal with mean value of -35.5 ‰ and amplitude of 16 ‰). (a) Vertical homogeneous temperature profile; (b) $\delta^{18}O$ profile at the beginning and end of the simulation; (c) Deviation of the $\delta^{18}O$ relative to the original profile, for 10 dates; (d) Evolution of the deviation to the original profile of $\delta^{18}O$.

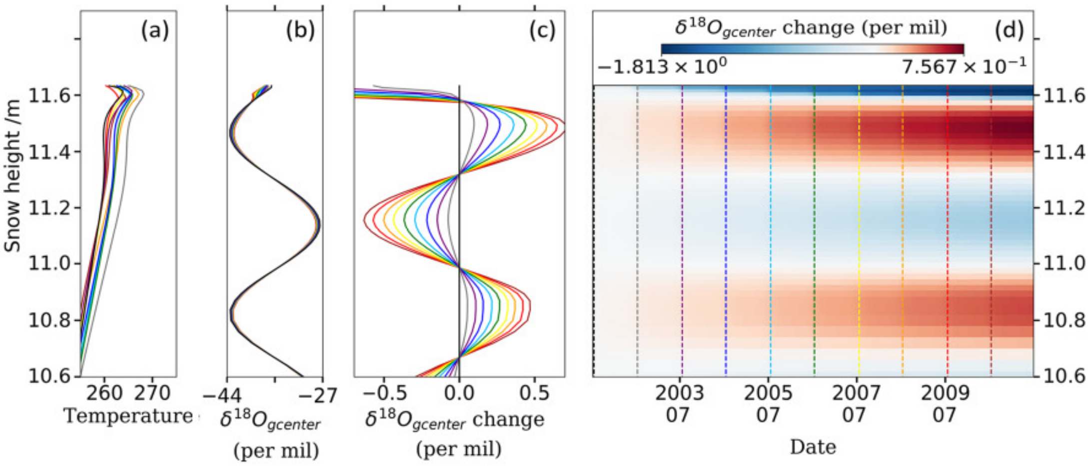

Figure 3. Simulation of the attenuation of the seasonal $\delta^{18}O_{gcenter}$ variation caused by diffusion in vapor phase over 10 years (with temperature evolution, original signal with mean value of -35.5 ‰ and amplitude of 16 ‰). (a) Vertical temperature profile for each summer; (b) $\delta^{18}O_{gcenter}$ profile for each summer; (c) Deviation of the $\delta^{18}O$ relative to the original profile, for each summer; (d) Evolution of the deviation to the original profile of $\delta^{18}O_{gcenter}$.

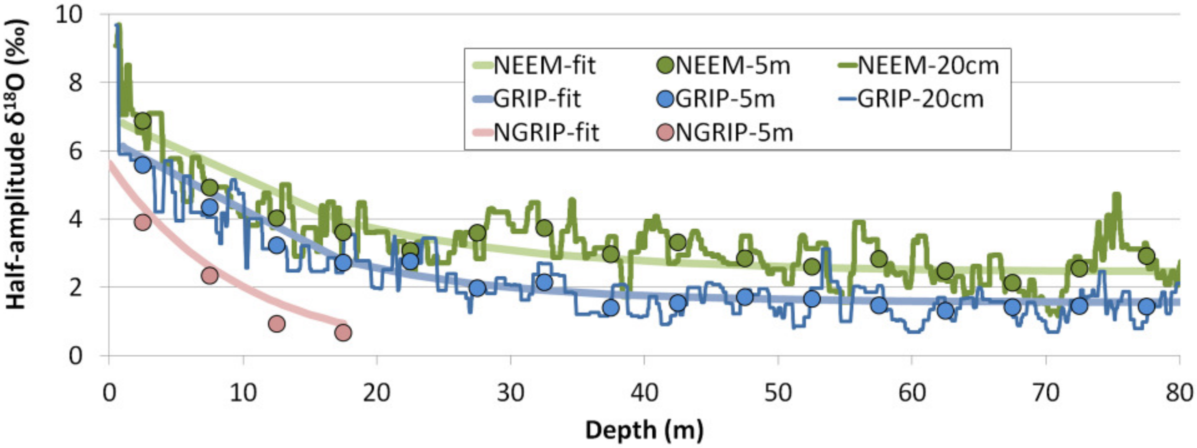

Figure 4. Evolution of the δ^{18}O half-amplitude with depth in shallow cores at NEEM, GRIP and NGRIP (Steen-Larsen et al., 1040 2011 and Masson-Delmotte et al., 2015; White et al., 1997; Johnsen et al., 2000). The attenuation of the half-amplitude values with depth was fitted using an exponential equation (Eq. 21):

$$A = A0 \cdot \exp(-\gamma \cdot z) - b \quad (21)$$

With A0=4.976 ‰; γ=0.08094; b=-1.56 ‰ at GRIP, and A0=4.685 ‰; γ=0.06622; b=-2.44 ‰ at NEEM.

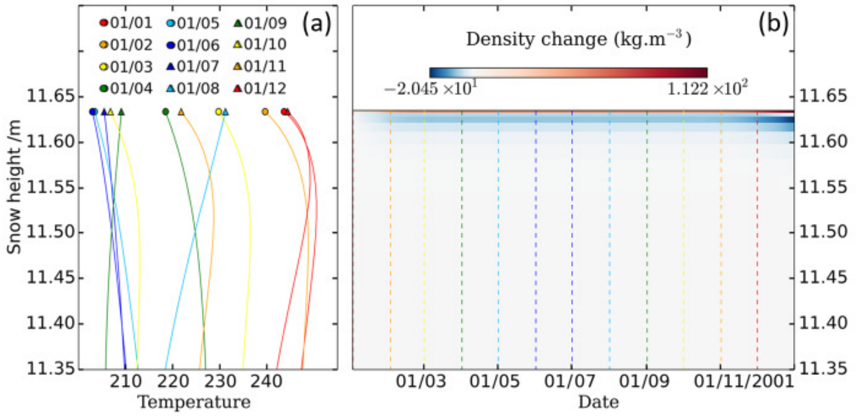

Figure 5. Change in snow density caused by vapor transfer over one year (cumulative). (a) Temperature profile on the first day of each month, around 8 pm. The 1st of August corresponds to a short-term warm event within winter. (b) Evolution of the snow densities. During summer, the first layer is gaining water whereas the layers immediately below (11.58 to 11.63 m) are losing water. Thus the vapor departure region is not exactly at the top of the snowpack in this simulation. Further down, layers are once again gaining water. During winter, temperature gradients are generally reversed, but the amount of vapor is too small to visibly affect the layer densities (for instance, the warming of Aug., 1st leads to a density loss of only 0.2 kg/m^3 in the first layer).

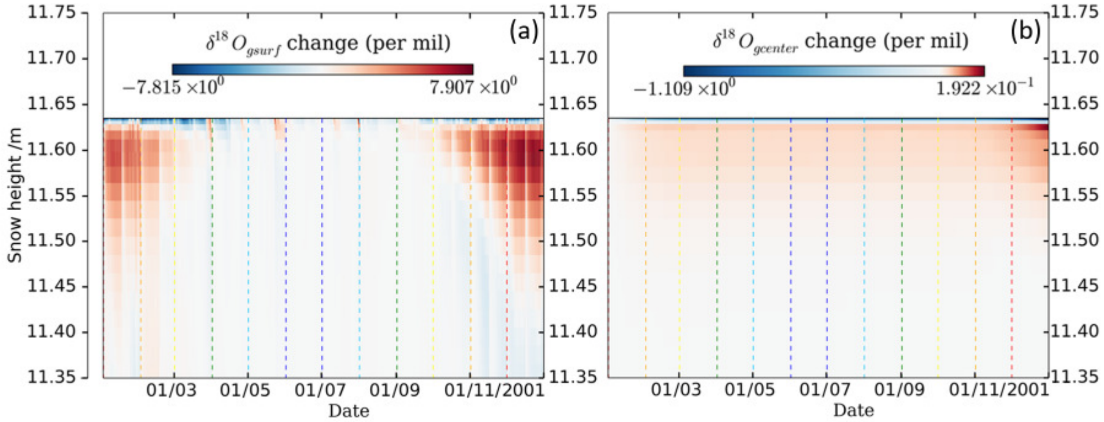

Figure 6. Change of δ^{18}O values caused by vapor transfer from January to December 200. (a) grain surface; (b) grain center. For both grain compartments: δ^{18}O values change as a result of vapor transport and therefore maximum change occurs during summer. The first layer that receives water has δ^{18}O values that decrease during summer, whereas δ^{18}O values increase in the layers immediately below (zone of water export). Further down (around 11.35 m) the δ^{18}O values decrease (arrival of ^{18}O-depleted vapor). During the winter, short-lived warm events (like the one on the 1st of August) lead to small changes in the δ^{18}O values (the first layer δ^{18}O increases). This is more visible for grain surface than for grain center.

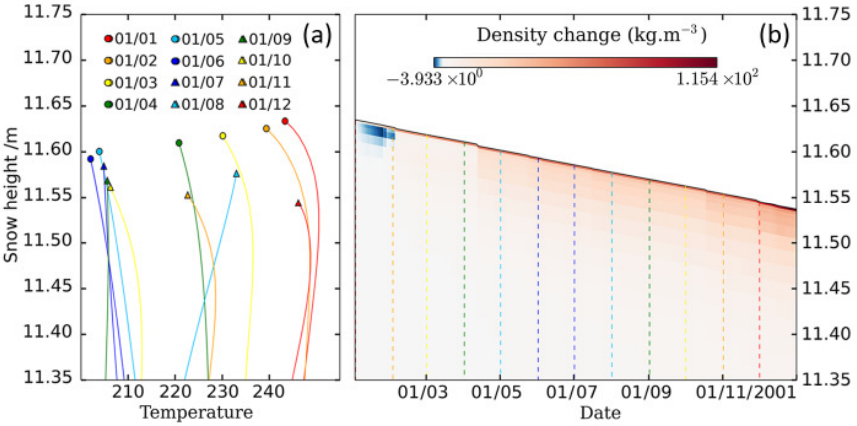

Figure 7. Evolution of the snow density over one year in a case with homogeneous compaction and wind drift, but without precipitation. The density change is taken as the difference relative to the first day for each layer (layer 1 is compared to layer 1, layer 5 to layer 5 etc…), even if they are not at the same height; thus density change may be overestimated compared to "horizontal" density change).

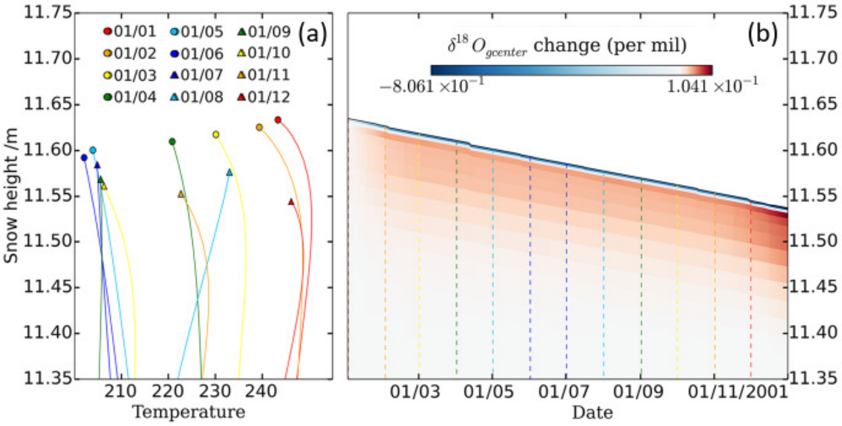

Figure 8. Cumulative change in $\delta^{18}O_{gcenter}$ values (vapor transport, compaction and wind drift active).

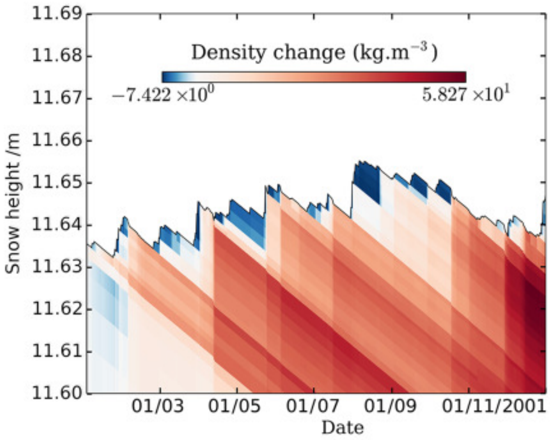

1075 **Figure 9.** Snow density change (relative to original density profile at t0) over one year: precipitation (snowfall) active, compaction (wind and weight) active, vapor transfer active.

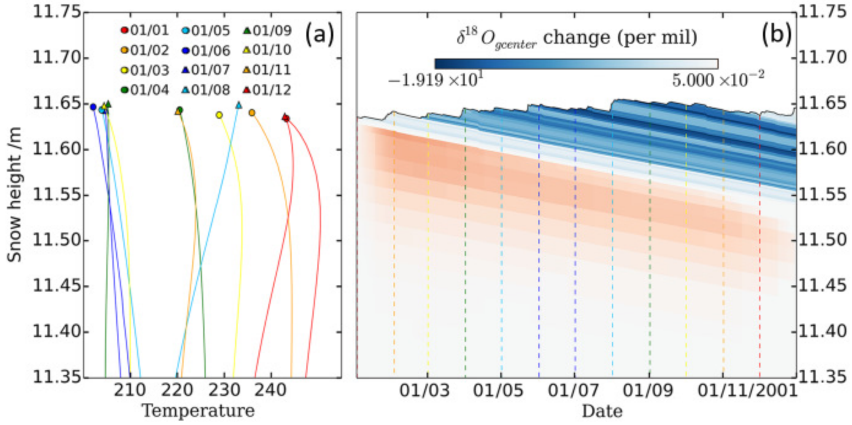

Figure 10. Cumulative change of δ^{18}O values at the grain center (relative to t0) over 6 months. Simulation with snowfall 1080 with varying δ^{18}O (function of T_{air}), vapor transport active, wind and weight compaction active.

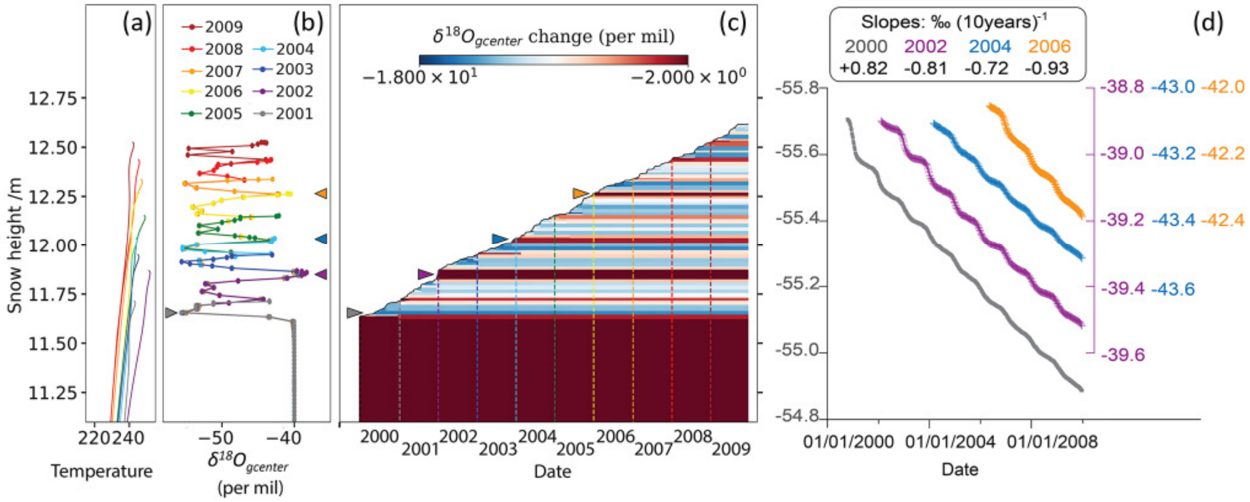

Figure 11. Evolution of $\delta^{18}O_{gcenter}$ values as a result of snowfall and vapor transport over 10 years (compaction is inactive; merging between layers is allowed but limited). (a) Temperature profiles at mid-January for each year. (b) $\delta^{18}O_{gcenter}$ profile at mid-January for each year. (c) Repartition of $\delta^{18}O$ values (expressed relative to -40‰) as a function of time and depth. (d) Evolution of $\delta^{18}O_{gcenter}$ values after burial for 4 selected layers (deposited in winter 2000, and summer 2002, 2004, 2006). Note that we do not present the evolution of snow composition in the first year after deposition because the thin snow layers resulting from precipitation are getting merged.

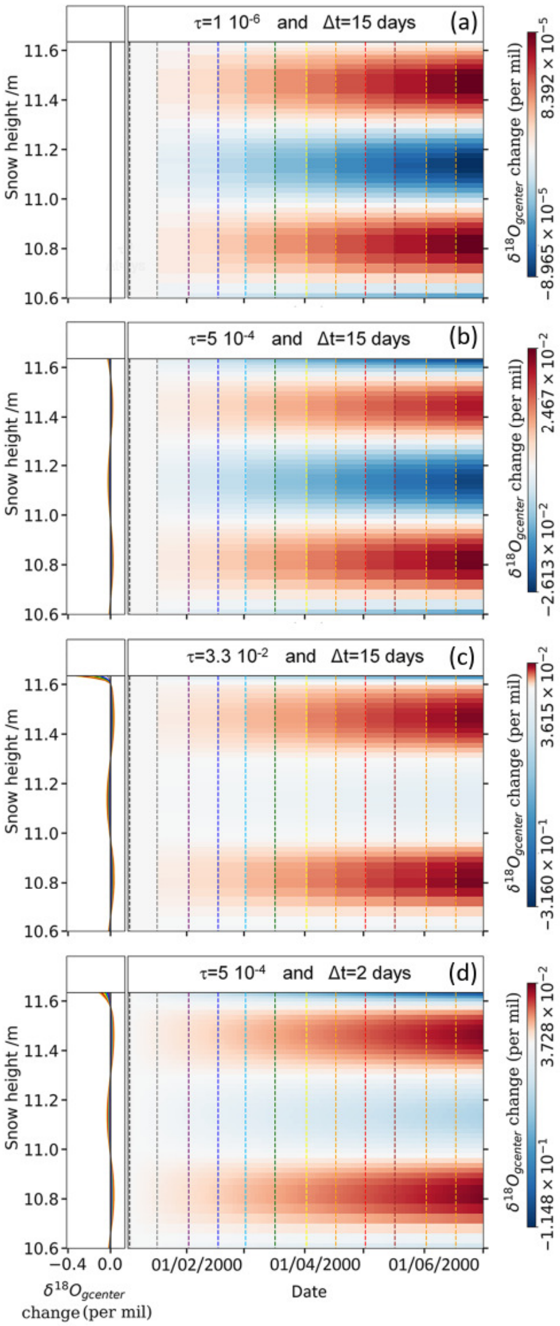

Figure 12. Test of the sensitivity of the model to the ratio of mass between surface and grain center compartments and to the interval of mixing between the two compartments (GRIP).

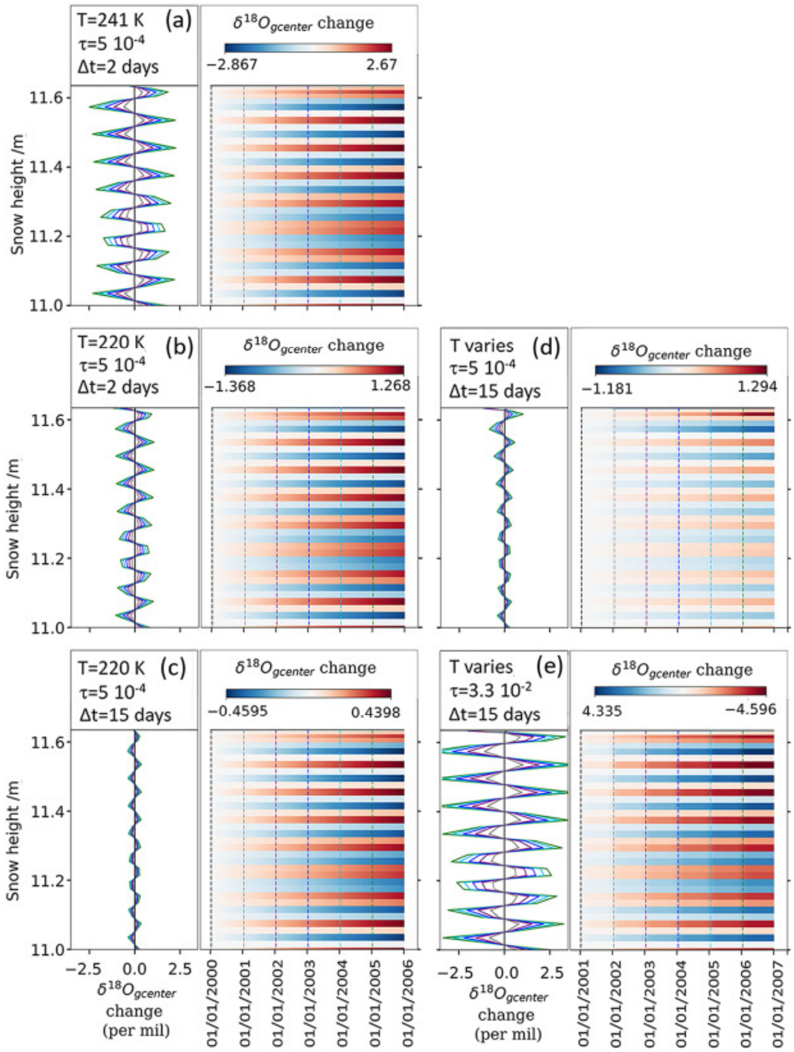

Figure 13. Test of the sensitivity of the model to the ratio of mass between surface and grain center compartments and to the interval of mixing between the two compartments (Dome C).